Excess volume, isothermal compressibility, isentropic compressibility and speed of sound of carbon dioxide+n-heptane binary mixture under pressure up to 70 MPa. II. Molecular simulations

Abdoul Wahidou Saley Hamani, Hai Hoang, Thieu Quang Quoc Viet, Jean-Luc Daridon, Guillaume Galliero

Excess volume, isothermal compressibility, isentropic compressibility and speed of sound of carbon dioxide + n-heptane binary mixture under pressure up to 70 MPa. II. Molecular Simulations

Abdoul Wahidou Saley Hamani[1], Hai Hoang[2], Thieu Quang Quoc Viet[3], Jean-Luc Daridon[1], Guillaume Galliero[1*]

[1]Laboratoire des Fluides Complexes et leurs Reservoirs, LFCR UMR 5150, Universite de Pau et des Pays de l'Adour, E2S UPPA, CNRS, TOTAL, Pau, France

[2]Institute of Fundamental and Applied Sciences, Duy Tan University, 10C Tran NhatDuat Street, District 1, Ho Chi Minh City 700000, Vietnam

[3]Department of Chemical Engineering, College of Technology, Can-Tho University Campus II, 3/2 street, Ninh Kieu district, Can Tho city, Vietnam

*** Corresponding Author: guillaume.galliero@univ-pau.fr**

Abstract

Molecular simulations have been performed in this work to provide a microscopic understanding of the experimental results of asymmetric supercritical binary mixtures of carbon dioxide and n-heptane published in the first article of the series [Bazile *et al.* J. Supercrit. Fluids 140, 218 (2018)]. Interestingly, molecular simulations results compared well with experimental data on density, isothermal compressibility, speed of sound, isentropic compressibility and the corresponding excess properties. In addition, using Kirkwood-Buff theory, computed partial molar volumes are found to be consistent with those obtained indirectly from experimental data. In particular, the negative value of partial molar volume of n-heptane at infinite dilution close to CO_2 critical conditions is well captured, confirming the occurrence of a clustering phenomenon at such conditions. Last, computed properties of the cluster indicates a weak cluster with a radius of about 3 nm and a residence time of the CO_2 molecules in the cluster of about 25 ps.

Keywords: Thermophysical properties, Carbon Dioxide, Cluster**s**, Asymmetric mixture, Molecular Simulations, Kirkwood-Buff Theory.

I. Introduction

In the first article of the series [1], an experimental investigation of volumetric and acoustic properties of a simple proxy to carbon dioxide enhanced oil recovery systems consisting of a binary mixture of carbon dioxide + n-heptane (nC_7) has been presented. The measurements were performed for two isotherms (303.35 and 313.25 K) at pressures from 10 to 70 MPa, i.e. including thermodynamic states in the vicinity of the CO_2 critical point. The experimental results highlighted the highly non-ideal behavior of the mixture in conditions close to the CO_2 critical point. In particular, the partial molar volume of n-heptane at infinite dilution, that was computed by fitting the molar volume data at fixed pressure and temperature, was found to be noticeably negative close to the critical point of CO_2. However, because of a lack of data due to experimental limitations [1], the molar volume data used in the fitting process was not containing the values for mole fractions of nC_7 ranging from 0.00 to 0.10 where the molar volume significantly varies with mole fraction. This may have led to inaccurate determination of the partial molar volume as pointed out by various authors [2-3]. Therefore, and this is one goal of this work, it would be relevant to propose an alternative to compute the partial molar volume of such systems.

The negative value of the nC_7 partial molar volume at infinite dilution was attributed to a clustering phenomenon occurring in the mixture [4-9]. This phenomenon, usually interpreted as the organization of solvent molecules (here CO_2) in "cluster" around the solute (here nC_7) molecules, corresponds to an augmentation of the solvent density around solute molecule [8-9]. To quantify the clustering phenomenon, a quantity, called "cluster size", could be estimated from the partial molar volumes [7]. This is what has been done in our previous experimental work [1], obtaining a value of the cluster size of about 8 CO_2 molecules at an experimental condition close to the CO_2 critical point (T=313K and P=10.11MPa). However, the exact microscopic nature of the clustering effect and the definition of the "cluster size" has not, to the best of our knowledge, been explored for molecular fluids such as those studied here [1]. This is the main goal of the proposed study.

Molecular simulation has shown to be a useful tool to provide microscopic insights on fluid mixtures at the molecular level [10-13]. Among others, this tool has been used to elucidate microscopic characteristics of clustering in supercritical solutions [14-16]. In addition, molecular simulation combined with the fluctuation theory allows a direct computation of thermodynamic derivative properties such as isothermal compressibility and partial molar volumes, whereas, experimentally, these quantities are usually deduced indirectly from a fitting procedure on density data. [12, 17-21]. Furthermore, with progresses in the definition of the

force fields used to describe the molecular interactions, molecular simulations are now able to predict thermodynamic properties of fluids in good agreement with the experiments [22-27]. Thus, molecular simulation is fully adapted for the purposes of this work which are to complement experimental data and to provide a microscopic interpretation of the results obtained in [1], in particular those related to the clustering effect.

The article is structured as follows. In Sect. II, details on the molecular simulations are provided. Methods used to compute the thermodynamic properties are introduced in Sect. III. Simulation results on the thermodynamic properties and the microscopic analysis of CO_2 clusters are presented and discussed in Sect. IV. Finally, the main outcomes of this study are summarized in Sect. V, which forms the conclusion.

II. Molecular Modeling and Simulations

2.1. Molecular Modeling

All the molecules of carbon dioxide and n-heptane binary mixture have been modeled by a Mie Chain Coarse Grained (MCCG) force field developed in [27], following the ideas proposed by Mejia *et al.* [28]. This coarse grained force field has been shown to successfully predict the thermophysical properties of these kind of components [27, 29-31] with a reasonable computational cost as it is usually the case with coarse grained force fields [32-33].

The molecular representation with MCCG consists in using homo-nuclear chains composed of N freely jointed spheres in which two adjacent particles in a chain are linked by a bond with a constant length. Interactions between two non-bonded spheres i and j are described by the Mie λ-6 potential [34]:

$$u_{Mie}(r_{ij}) = \left(\frac{\lambda_{ij}}{\lambda_{ij}-6}\right)\left(\frac{\lambda_{ij}}{6}\right)^{6/(\lambda_{ij}-6)} \varepsilon_{ij}\left[\left(\frac{\sigma_{ij}}{r_{ij}}\right)^{\lambda_{ij}} - \left(\frac{\sigma_{ij}}{r_{ij}}\right)^{6}\right] \quad (1)$$

where ε_{ij}, σ_{ij}, λ_{ij} and r_{ij}, are respectively the potential well depth, the collision diameter, the exponent characterizing the repulsive interactions between non-bonded spheres and the distance between two spheres. The MCCG parameters used for both carbon dioxide and n-heptane are reported in Table I. The bond length is fixed to be equal to σ_{ij}.

Table I. Mie Chain Coarse Grained (MCCG) parameters of Carbon dioxide and n-heptane [27].

Molecules	N	σ_{ii} (Å)	ε_{ii}/k_B [K]	λ_{ii}
Carbon Dioxide	2	2.861	211.54	16.93
n-Heptane	3	4.049	294.29	14.03

For weakly asymmetric mixtures, Hoang et al. [27] proposed to use the classical Lorentz-Berthelot (LB) combining rules for σ_{ij} and ε_{ij} as:

$$\sigma_{ij} = \frac{(\sigma_{ii}+\sigma_{jj})}{2} \quad (2)$$

$$\varepsilon_{ij} = \sqrt{\varepsilon_{ii}\varepsilon_{jj}} \quad (3)$$

And, the repulsion exponent of the cross-interactions, λ_{ij}, is evaluated using an arithmetic average as:

$$\lambda_{ij} = \frac{\lambda_{ii}+\lambda_{jj}}{2} \quad (4)$$

Such combining rules was found to be provide reasonable results for noble gases mixtures as well as normal alkanes mixtures [27, 29-31]. However, when dealing with an asymmetric mixture of CO_2 + nC_7, in which the CO_2 molecules have a quadrupole moment, the classical LB combining rules, i.e. Eqs. 2 and 3, are usually insufficient to accurately describe the cross interaction mixture parameters [35]. To check this point, we have performed a preliminary study to assess the capability of these combining rules for predicting equilibrium phase composition and Henry's law constant of CO_2 in liquid nC_7, the latter being defined [36] as:

$$H_{CO_2} = \lim_{x_{CO2}\to 0}\left[\frac{f_{CO2}^{liq}}{x_{CO2}}\right] = \rho_{nC7}^{*}\, k_B T exp(\frac{\mu_{CO2}^{ex}}{k_B T}) \quad (5)$$

where f_{CO2}^{liq} and x_{CO2} are respectively the fugacity and the mole fraction of CO_2 in liquid nC_7, ρ_{nC7}^{*} the number density of the liquid n-heptane and μ_{CO2}^{ex} is the excess chemical potential of CO_2 in the liquid nC_7. To do so, phase equilibrium properties have been computed by carrying out Gibbs Ensemble Monte Carlo simulations [37-38] during which μ_{CO2}^{ex} has been estimated by using the Widom method [39-40].

Figs. 1 and 2 show comparisons between molecular simulation and experimental results [41]. It appears clearly that the combining rules defined by Eqs. 2-4 do not correctly capture the cross interactions of the studied mixture. To overcome this problem, the potential well depth combing rule given by Eq. 3 was corrected using a binary interaction parameter k_{ij}:

$$\varepsilon_{ij} = (1 - k_{ij})\sqrt{\varepsilon_{ii}\varepsilon_{jj}} \quad (6)$$

assuming that fluid-phase equilibria are dominated by the energetic contributions to the interactions [35, 42-43]. The correction protocol consists in choosing a k_{ij} value leading to the right prediction of the aforementioned phase equilibrium properties. To determine the appropriate binary coefficient, we have employed a minimization method [44] based on the

deviations between experimental and numerical data on phase composition and Henry's law constant.

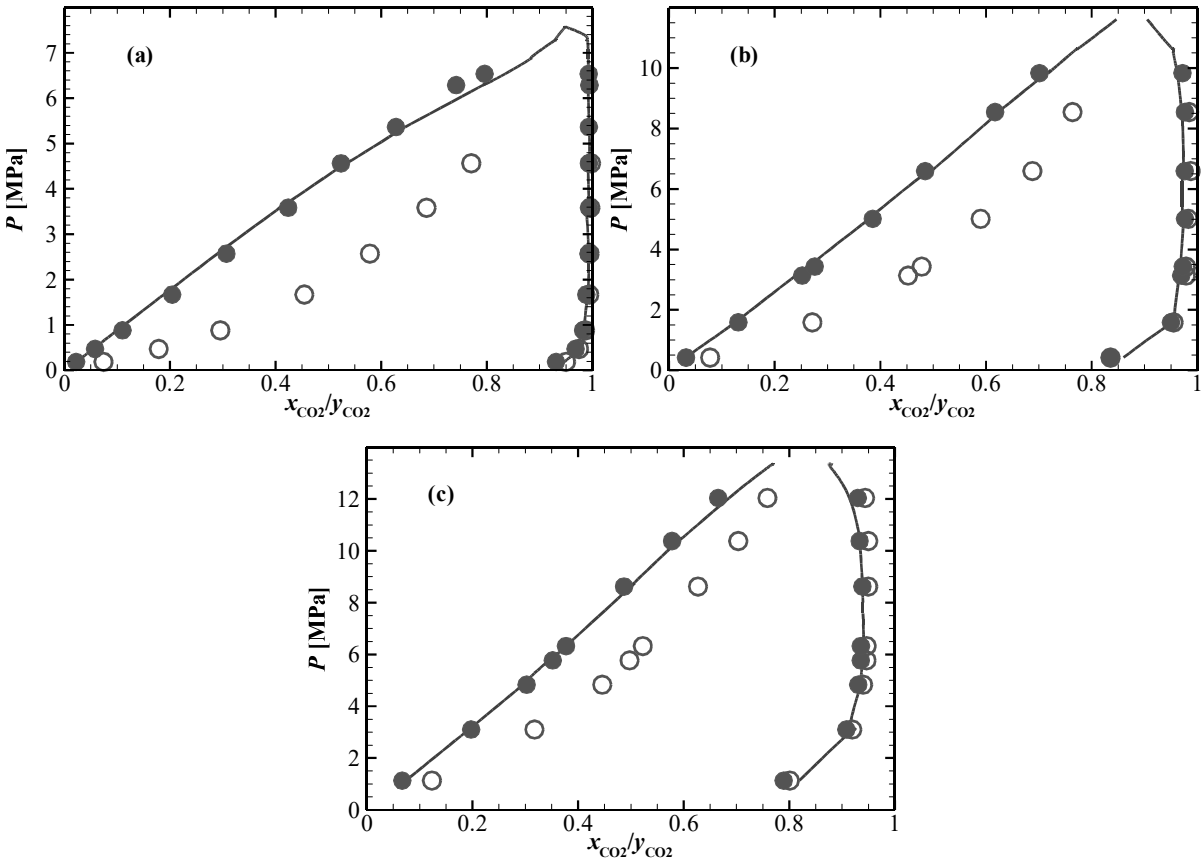

Figure 1. Equilibrium phase compositions for the carbon dioxide + n-heptane binary systems at different temperatures. (a): T=310.65 K. (b): T=352.60 K. (c): T=394.26 K. Comparison between experimental data (lines) provided by Kalra et al. [41] and GEMC simulation results with (solid circles) and without (open circles) binary coefficient correction k_{ij}.

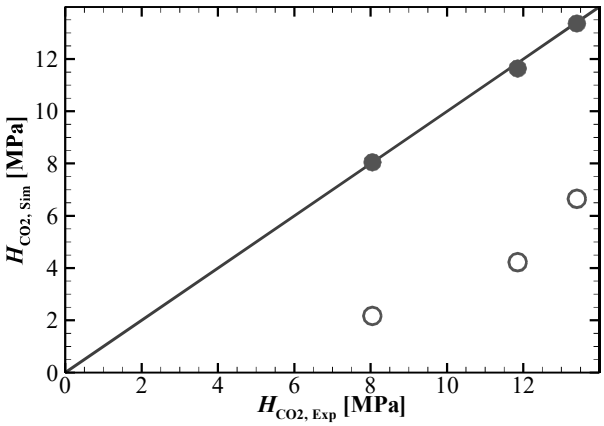

Figure 2. Henry's law constants obtained from molecular simulation as a function of experimental values taken from Kalra et al. [41] for carbon dioxide + n-heptane mixture.

Comparison between simulation results with (solid circles) and without (open circles) binary coefficient correction k_{ij}.

Results shown in Figs. 1 and 2 indicate that k_{ij} equals 0.138, 0.128 and 0.113 at T=310.6, 352.6 and 394.3K, respectively, provides both VLE and Henry's law constant in good agreement with experimental data [41]. Then, these values were fitted as a linear function of temperature [45] to determine k_{ij} at the temperatures of interest, i.e. T=303.35 and 313.25K. This has led to k_{ij} equal to 0.140 and 0.138 for T=303.35 and 313.25K, respectively.

2.2. Molecular Simulations.

A. Monte-Carlo simulations.

To compute equilibrium thermodynamic properties such as density, isothermal compressibility, speed of sound and isentropic compressibility, we performed Monte Carlo simulations in the isobaric isothermal ensemble (*NPT*) [10-12] using an in-house code. The simulation systems were composed of cubic boxes containing at least 500 molecules for conditions far from the critical point of CO_2 (i.e. $x_{CO2} \leq 60$ mol% and $P \geq 40.23$ MPa) and 1000 molecules for other systems. The periodic boundary conditions were applied in all the directions. The Mie λ-6 potential was truncated at a cut-off radius r_C and the long range corrections were included [10-12]. Details about chosen r_C values are provided in the following section.

To generate new configurations, four MC moves were implemented: volume change, molecular translation, molecular rotation and configurational-bias MC partial regrowth [10-12]. In these simulations, the system was first equilibrated by carrying out at least 3.10^7 MC moves followed by a period of more than 2×10^8 moves during which the sampling was carried out to determine the thermodynamic properties. During the equilibration stage, the maximum amplitudes of the three first MC moves were adjusted so that their acceptance rates are approximately equal to 50% [10-12]. Error bars have been computed from the sub-block method [10].

B. Molecular Dynamics Simulations.

To compute additional microscopic properties such as the radial distribution functions and residence times of CO_2 molecules around the n-heptane molecule, Molecular Dynamics (MD) simulations in *NPT* ensemble [10-12] have been performed by using an in-house code. For that purpose, the simulation systems were made up of cubic boxes composed of at least 3000 molecules for conditions far from the critical point of pure CO_2 (i.e. $x_{CO2} \leq 60$ mol% and

P ≥ 40.23 MPa) and at least 5000 molecules for other mixtures. In particular, for the MD simulations performed at "infinite dilution" of nC_7, the system was composed of at least 5000 molecules of CO_2 and 1 molecule of n-heptane. Classical periodic boundary conditions were applied in all directions.

During MD simulations, the equations of motion were integrated using the velocity-Verlet algorithm [46]. The temperature and pressure were kept constant using a Berendsen thermostat and barostat, respectively [47]. The classical RATTLE algorithm was employed to constrain the bond length [48]. All MD simulations consist of two steps. First, the systems were equilibrated for 2.10^6 time steps. Then, the samplings were carried out during at least 6.10^6 time steps. Error bars have been computed from the sub-block method, except for the infinite dilution systems for which they were calculated from at least 10 independent MD simulations to improve the statistical uncertainties [10].

Similarly to MC simulations, the non-bonded Mie λ-6 potential was truncated at a cut-off radius r_C and long range corrections were included [10-12]. It should be noticed that, even if the long range corrections are included, the cut-off radius has a strong effect on thermodynamic properties of the mixtures close to the critical point [49]. This is because the correlation lengths of the near-critical fluctuations are known to diverge when approaching the critical point [49-50]. Therefore, to choose adequate values of r_C, we have investigated its effect on the simulation of density. Results have shown that a r_C value higher or equal to $7\sigma_{ij}$ was sufficient for the thermodynamic condition that is the most impacted by the critical point vicinity, i.e. the one corresponding to the highest value of the isothermal compressibility which is at x_{CO2}=1.0, *T*=313.25K, *P*=10.11MPa [1]. Then, we have evaluated the range of conditions (both in pressure and in composition) for which a usual lower cut-off radius ($r_C = 4\sigma_{ij}$) could yield results consistent with those provided with ($r_C = 7\sigma_{ij}$). It has been obtained that $r_C = 4\sigma_{ij}$ is sufficient to provide consistent densities for the following thermodynamic conditions *T*=313.25K, *P*=10.11MPa, x_{CO2}≤0.6 and *T*=313.25K, *P*≥40.23 MPa, x_{CO2}=1.0. To sum up, for both *T*=303.35 K and 313.25 K, we have used $r_C = 7\sigma_{ij}$ for thermodynamic conditions respecting 10.11≤*P*<40.23 and 0.6<x_{CO2}≤1.0, so-called conditions close to the critical point, and $r_C = 4\sigma_{ij}$ for the other thermodynamic conditions, so-called conditions far from the critical point. Such values of r_C have been used in both MC and MD simulations to compute both the thermodynamic and the structural properties.

III. Thermodynamics Properties Computations

3.1. Classical computations

Density was directly computed by taking the average of its values during the MC simulations as [10, 12]:

$$\rho = \langle \frac{\sum_i N_i \times M_i}{V} \rangle \quad (7)$$

where, N_i and M_i are number of molecules and molecular mass of the i^{th} compound, respectively, V is the volume, and $\langle ... \rangle$ denotes an ensemble average over MC moves.

The isothermal compressibility was also directly estimated from the MC simulations thanks to the fluctuation theory [10, 12, 17, 51] using:

$$\kappa_T = -\frac{1}{\langle V \rangle}\left(\frac{\partial \langle V \rangle}{\partial P}\right)_T = \frac{1}{\langle V \rangle k_B T}(\langle V^2 \rangle - \langle V \rangle^2) \quad (8)$$

where, k_B is the Boltzman constant.

The isentropic compressibility and the speed of sound, whose direct calculation during the simulations is not straightforward for molecular fluids, were deduced from other thermodynamic properties via classical thermodynamic relations [52] as:

$$k_s = \kappa_T - \frac{TM\alpha_P^2}{\rho c_p} \quad (9)$$

$$w = \frac{1}{\sqrt{\rho(\kappa_T - \frac{TM\alpha_P^2}{\rho c_p})}} \quad (10)$$

where, α_p is the isobaric thermal expansion and c_p is the molar isobaric heat capacity. These two last quantities were obtained from the simulations by using the fluctuation theory [17]. The isobaric thermal expansion was computed by:

$$\alpha_P = \frac{1}{\langle V \rangle}\left(\frac{\partial \langle V \rangle}{\partial P}\right)_T = \frac{1}{\langle V \rangle k_B T^2}\left(\langle V\widehat{H} \rangle - \langle V \rangle \langle \widehat{H} \rangle\right) \quad (11)$$

where, $\widehat{H}$ is the configurational enthalpy: $\widehat{H} = U^{ext} + U^{int} + PV$, U^{ext} and U^{int} are the intermolecular and intramolecular potential energy, respectively. Regarding the molar isobaric heat capacity c_P, since the kinetic energy is not considered in MC simulations, it is decomposed in an ideal and residual isobaric heat capacities as follows [17]:

$$c_P = c_P^{id} + c_P^{res} \quad (12)$$

where c_P^{id} is the ideal molar heat capacity obtained from the NIST database [53] and c_P^{res} is the residual heat capacity estimated from the simulations [17] as:

$$c_P^{res} = \frac{N_a}{k_B N T^2}\left(\langle U^{ext}\widehat{H} \rangle - \langle U^{ext} \rangle \langle \widehat{H} \rangle\right) + \frac{N_a P}{k_B N T^2}\left(\langle V\widehat{H} \rangle - \langle V \rangle \langle \widehat{H} \rangle\right) - N_a k_B \quad (13)$$

where N_a is the Avogadro number.

The radial distribution functions (RDF), which provide information on the structure of the studied fluid, were directly computed from the MD simulations [10] as:

$$g_{\alpha\beta}(r) = \langle \frac{V}{N_\alpha} \times \frac{1}{N_\beta} \sum_{i\in\alpha}^{N_\alpha} \sum_{j\in\beta}^{N_\beta} \frac{\delta(r_{ij}-r)}{4\pi r^2} \rangle \quad (14)$$

where, $g_{\alpha\beta}$ is the RDF of species β around species α, δ is the Dirac distribution function, N_α and N_β are the numbers of molecules of species α and β, respectively.

3.2. Computations from the Kirkwood-Buff Theory

Interestingly, in addition to the usual approach, Eq. 8, the isothermal compressibility can be alternatively computed from the microscopic structure thanks to the Kirkwood-Buff theory [54] using:

$$\kappa_T = \frac{1+c_\alpha G_{\alpha\alpha}+c_\beta G_{\beta\beta}+c_\alpha c_\alpha (G_{\alpha\alpha}G_{\beta\beta}-G_{\alpha\beta})^2}{k_B T(c_\alpha+c_\beta+c_\alpha c_\beta (G_{\alpha\alpha}+G_{\beta\beta}-2G_{\alpha\beta}))} \quad (15)$$

where c_α and c_β are the molar concentration of species α and β, respectively, and $G_{\alpha\beta}$ is the Kirkwood-Buff Integral (KBI) between species α and β that is defined as:

$$G_{\alpha\beta} = 4\pi \int_0^\infty \left[g_{\alpha\beta}^{\mu VT}(r) - 1 \right] r^2 dr \quad (16)$$

where $g_{\alpha\beta}^{\mu VT}$ is the RDF of species β around α in the grand canonical μVT ensemble. As can be seen from this expression, Eq. 16, KBI has unit of volume per molecule and quantifies the excess (or deficiency) of species α around species β relatively to a homogenous (random) distribution, i.e. when $g_{\alpha\beta}^{\mu VT}(r) = 1$.

The Kirkwood-Buff theory also provides a formula to directly calculate the partial molar volume v_α from the KBI as [54]:

$$v_\alpha = \frac{1+(G_{\beta\beta}-G_{\alpha\beta})c_\beta}{c_\alpha+c_\beta+c_\alpha c_\beta (G_{\alpha\alpha}+G_{\beta\beta}-2G_{\alpha\beta})} \quad (17)$$

This direct way to compute the partial molar volume is of great interest, as it is often indirectly obtained from a fitting procedure of volumetric data, which may induce important errors [55-57].

However, it is worth pointing out that the calculation of KBI, Eq. 16, from the RDFs obtained from molecular simulations is not straightforward and this explains why Kirkwood-Buff theory is not yet widely employed in the molecular simulations community. The difficulties in computing Eq. (16) are due to two main reasons. First, $g_{\alpha\beta}^{\mu VT}(r)$ of a molecular mixture in a dense state, as studied in this work, is often not accurately computed because of the difficulties in performing molecular simulations in the grand canonical ensemble, in particular when dealing with mixtures [10-11]. Second, the molecular simulations are carried

out on finite systems [10-11] and so the integral in Eq. 16 cannot be computed over an infinite volume as it should.

In this work, instead of determining $g_{\alpha\beta}^{\mu VT}(r)$ directly from molecular simulations in the grand canonical ensemble, we have first computed the RDF in the NPT (or NVT) ensemble, i.e. $g_{\alpha\beta}^{NPT}(r)$, and then corrected it to obtain an approximation of $g_{\alpha\beta}^{\mu VT}(r)$, as proposed in ref. [58], i.e.:

$$g_{\alpha\beta}^{\mu VT}(r) \approx g_{\alpha\beta}^{NPT}(r) \frac{N_\alpha\left(1-\frac{(4/3)\pi r^3}{V}\right)}{N_\alpha\left(1-\frac{(4/3)\pi r^3}{V}\right)-\Delta N_{\alpha\beta}(r)-\delta_{\alpha\beta}} \quad (18)$$

with

$$\Delta N_{\alpha\beta}(r) = 4\pi \int_0^r \rho_\beta \left[g_{\alpha\beta}^{NPT}(r') - 1\right] r'^2 dr' \quad (19)$$

where $\Delta N_{\alpha\beta}(r)$ is the excess or depletion number of particles of type α within a sphere of radius r around particles of type β and ρ_β the number density of particle of type β.

For the estimation of the integral in Eq. 16, we have first computed the KBI for different finite volumes, and then extrapolated it to the infinite volume limit [58-60]. The KBI for the finite volumes proposed by Krüger et al. [60] is defined as:

$$G_{\alpha\beta}^{V}(V) = \int_V \int_V \left[g_{\alpha\beta}^{\mu VT}(r) - 1\right] dr_1 dr_2 \quad (20)$$

This double integral can be reduced to a single one by introducing a weighting function $w(r)$ that is defined as:

$$w(r) = \frac{1}{V} \int_V \int_V \delta(r - r_{12}) dr_1 dr_2 \quad (21)$$

where $\delta(r - r_{12})$ is the Dirac delta function and $r_{12} = |r_1 - r_2|$ is the pair distance. The weighting function $w(r)$ is the one that is proportional to the probability of having two points inside the sub volume V separated by a distance r [60]. Then, $G_{\alpha\beta}^{V}$ is given by:

$$G_{\alpha\beta}^{V}(V) = G_{\alpha\beta}^{V}(R) = \int_0^{2R} w(r) \left[g_{\alpha\beta}^{\mu VT}(r) - 1\right] dr \quad (22)$$

For a spherical volume, the weighting function is defined [60] as:

$$w(r) = 4\pi r^2 (1 - 3r/4R + r^3/4R) \quad (23)$$

Given the variation in $G_{\alpha\beta}^{V}(R)$ with R, $G_{\alpha\beta}$ is approximated as:

$$G_{\alpha\beta} = \lim_{R\to\infty} G_{\alpha\beta}^{V}(R) = \lim_{1/R\to 0} G_{\alpha\beta}^{V}(R) \quad (24)$$

It has been shown that $G_{\alpha\beta}^{V}(R)$ linerly varies with $1/R$ for small values of $1/R$ [21, 60]. This enables a linear extrapolation of $G_{\alpha\beta}^{V}(R)$ with $1/R$ to finally compute KBI as shown in Fig. 3.

It should be noted that the direct replacement of $g_{\alpha\beta}^{\mu VT}(r)$ by $g_{\alpha\beta}^{NPT}(r)$ does not provide good

values for the KBI, whereas the corrected $g_{\alpha\beta}^{NPT}(r)$, using Eq. 18, is able to yield good results, as shown in Fig. 3.

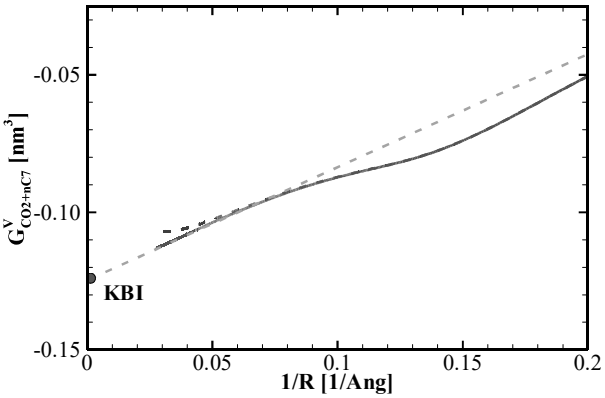

Figure 3: Dependence of $G_{\mathrm{CO2+nC7}}^{\mathrm{V}}$ with 1/R for the binary mixture of CO_2+nC_7 at x_{CO2}=0.40 T=303.35K and P=10.12 MPa. (Red color) solid line corresponds to the use of $g_{\mathrm{CO2+nC7}}^{\mu VT}(r)$ given by Eq. 18. (Blue color) dashed-dotted line corresponds to the use of $g_{\mathrm{CO2+nC7}}^{NPT}(r)$. (Green color) short-dashed line corresponds to the linear extrapolation used to deduce the KBI.

IV. Results and discussions

4.1. Thermodynamic Properties

In this section, we compare thermodynamic properties obtained from the molecular simulations and those provided from the experiments published in Ref. 1. To do so, MC simulations on pure carbon dioxide, n-heptane and their mixtures with CO_2 mole fractions of 20, 40, 60, 83.26, 88.49 mol% were carried out at the same conditions as experimental measurements, i.e. pressures ranging from 10 to 70 MPa and for two isotherms corresponding to 303.35 and 313.25 K. For further investigations, molecular simulations were also performed for two additional compositions (95 and 99 mol%) where experimental measurements on the speed of sound were not possible to achieve with our experimental devices [1, 61].

A. Density and derivative properties

Densities obtained from the MC simulations are reported in Table A. 1 of the Appendix. Compared to experimental results reported in the previous work [1], they are globally in good agreement with the experimental densities, see Fig. 4. In more details, simulation results remarkably matches experimental ones with absolute deviations (AD) that are not greater than 1% for conditions far from the critical point (i.e. $x_{CO2} \leq 60$ mol% and P ≥30 MPa), whereas the deviations from experimental data are much more pronounced for the conditions near the CO_2 critical point, reaching up to 4% for the pure CO_2 at T=313.15 K and P=10.11 MPa, see Fig. 4.

These observations indicate that the deviations mostly arise from the proximity to the CO_2 critical point, which is probably due to the difficulties to accurately describe this region with molecular simulations combined with the intrinsic limitations of the MCCG force field [12, 27].

Experimental results have shown a non-monotonic variation in the density with CO_2 content at P=10.11 MPa [1], which is well captured by the molecular simulations, as shown in Fig. 4. However, due to difficulties in experimental measurements [1], the experimental data do not include the values for CO_2 contents in the range of 88.49 to 100 mol% [1], where the variation of the density with the CO_2 content is the largest at P=10.11 MPa, see Fig. 4. Hence, to better describe this variation, we have performed MC simulations to compute the density at two additional CO_2 contents (95 and 99 mol%).

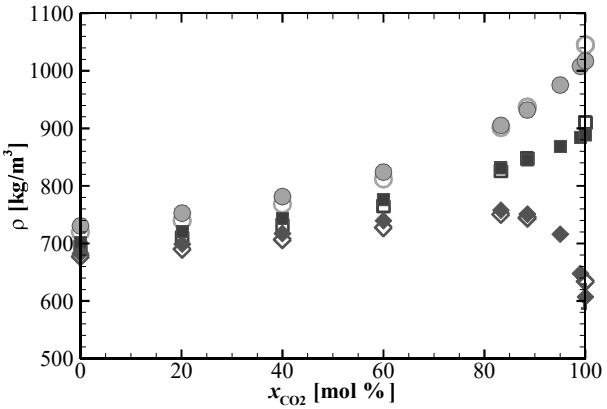

Figure 4. Comparison between variations in density with the CO_2 mole fraction obtained from experiments [1] (open symbols) and molecular simulations (solid symbols) at T=313.25 K and P=10.11MPa (diamonds), P=30.16MPa (squares) and P=70.54MPa (circles).

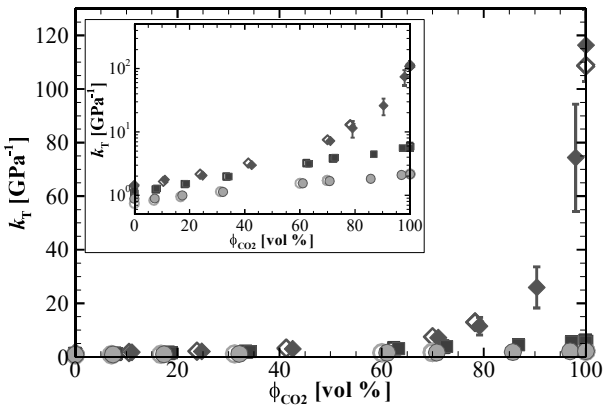

Figure 5. Comparison between variations in isothermal compressibility with CO_2 volume fraction obtained from experiments [1] (open symbols) and molecular simulations (solid

symbols) at T=313.25 K and P=10.11MPa (diamonds), P=30.16MPa (squares) and P=70.54MPa (circles). The inserted figure displays k_T in a logarithm scale.

In addition to density, MC simulations provide the isothermal compressibility values of the system by analyzing volume fluctuations thanks to Eq. 8. These data are given in Table A. 2 of the Appendix. This derivative property is rather well predicted by the MC simulations in comparison with the experiments. The AD varies between 0.5% for the pure n-heptane and 10% for the mixture with the highest CO_2 content at T=313.25K and P=10.11 MPa, see Fig. 5. These deviations are consistent with those on the density and are probably related to the limitations of the chosen force fields in the region around the CO_2 critical point and the difficulties in capturing accurately the density fluctuations in near critical conditions [49].

Despite the non-monotonic behavior of density with composition at T=313.25 K and P=10.11 MPa, isothermal compressibility deduced from experiments monotonously increases with the CO_2 content [1], see Fig. 5, as for all thermodynamic conditions studied in this work. Interestingly, this behavior is well captured by molecular simulations as shown in Fig. 5 in which the volume fraction of CO_2 used in x-axis corresponds to the ideal volume fraction defined [1] as:

$$\phi_{CO2} = \frac{x_{CO2} M_{CO2}}{\rho_{CO2} \sum_i x_i \frac{M_i}{\rho_i}} \quad (25)$$

where the subscript i denotes carbon dioxide and n-heptane. The use of the volume fraction as abscissa has been chosen because the isothermal compressibility of an ideal mixture is a linear function of the volume fraction [1]. It is also interesting to notice that the significant departure of k_T to linearity for the mixtures with a high CO_2 content, indicating non ideality, is well captured by the molecular simulations, see Fig.5.

In addition, the isentropic compressibility k_s and the speed of sound w were indirectly calculated from the standard thermodynamic relationships (Eqs. 9 and 10) using density, isothermal compressibility, isobaric thermal expansion and molar heat capacity directly taken from MC simulations. The computed data of k_s and w are provided in Tables A. 3 and A. 4 of the Appendix. Although this indirect method can lead to important expanded uncertainties [31], it provides the isentropic compressibility and the speed of sound in quantitative agreement with experimental results as shown in Figs 6 and 7. The AD is smaller than 20% for the isentropic compressibility, and it is of the order of 10% for the speed of sound. The largest deviations correspond to the mixture with the high CO_2 content. Furthermore, the simulation data of the two additional CO_2 contents of 95 and 99 mol%, where experiments were not possible to

perform with the pulse echoes technique used, emphasizes the interest of molecular simulations to explore conditions for which experiments are difficult to achieve [1, 61].

B. Excess Properties

To go further in our investigations using the simulation results, we have calculated excess volumetric and acoustic properties of the studied mixtures that are defined as:

$$y^E = y - y^{id} \tag{26}$$

where y denotes either V_m, κ_T, κ_S or w and the superscript id the corresponding ideal mixture properties estimated using the following equations :

$$V^{id} = \sum_i x_i \frac{M_i}{\rho_i} \tag{27}$$

$$\kappa_T^{id} = \sum_i \phi_i \kappa_{T,i} \tag{28}$$

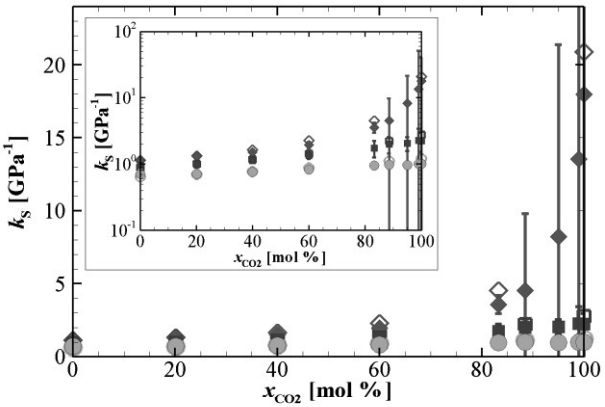

Figure 6. Comparison between variations in isentropic compressibility with CO_2 volume fraction obtained from experiments [1] (open symbols) and molecular simulations (solid symbols) at T=313.25K and P=10.11MPa (diamonds), P=30.16MPa (squares) and P=70.54MPa (circles). The inserted figure displays k_S in the logarithm scale.

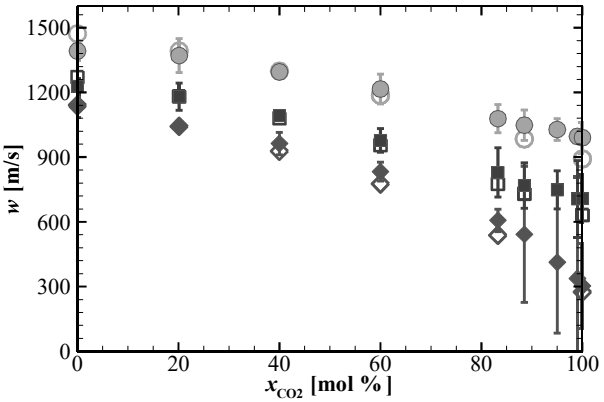

Figure 7. Comparison between variations in speed of sound with CO_2 mole fraction obtained from experiments [1] (open symbols) and molecular simulations (solid symbols) at T=313.25 K and P=10.11MPa (diamonds), P=30.16MPa (squares) and P=70.54MPa (circles).

$$\kappa_S^{id} = \sum_i \phi_i \kappa_{T,i} - \frac{\left(\sum_i x_i \frac{M_i}{\rho_i}\right)\left(\sum_i \phi_i \alpha_{p,i}\right)^2}{\sum_i x_i \frac{M_i T \alpha_{p,i}^2}{\rho_i\left(\kappa_{T,i} - \kappa_{S,i}\right)}} \tag{29}$$

$$w^{id} = \frac{\sum_i x_i \frac{M_i}{\rho_i}}{M \kappa_S^{id}} \tag{30}$$

where the subscript i denotes either CO_2 or nC_7 .

Evaluation of these excess properties is very important because they quantify the non-idealities of an asymmetric mixture [2]. Thus, this allows one to deeply check the capability of the molecular simulations to deal with the studied mixtures, from the mixing point of view alone. However, it is worth noticing that the excess properties determinations either from experiment and simulation may be affected by large errors bars, especially for properties such as κ_S^E and w^E.

Interestingly, it has been found that all excess properties are qualitatively and quantitatively well estimated by molecular simulations when compared to experimental data, as displayed in Fig. 8. These observations provide further evidence of the good capability of the MCCG force fields combined with modified Lorentz-Berthelot rule to describe the asymmetric mixture studied in this work, even close to critical conditions.

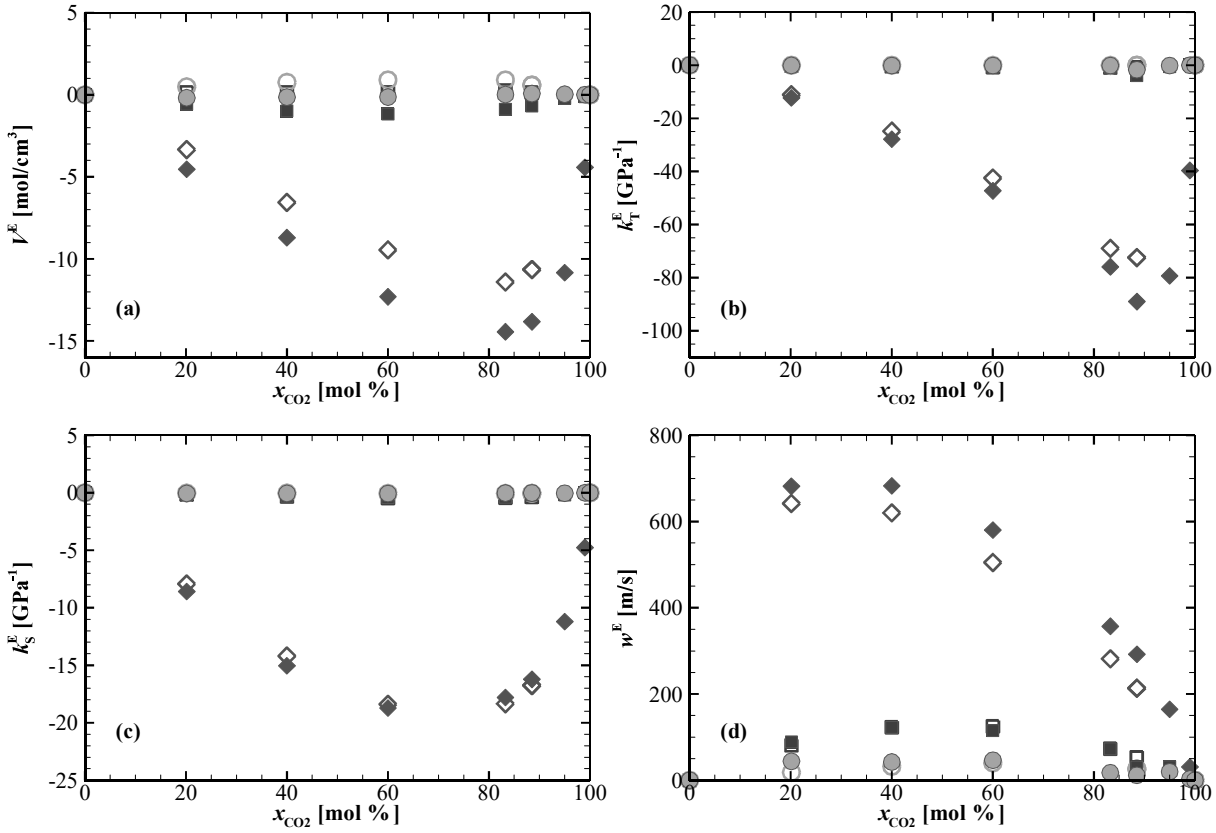

Figure 8. Comparison between variations in excess properties with CO_2 mole fraction deduced from experiments [1] (open symbols) and molecular simulations (solid symbols) at T=313.25 K and P=10.11MPa (diamonds), P=30.16MPa (squares) and P=70.54MPa (circles). (a): Excess molar volume. (b): Excess isothermal compressibility. (c): Excess isentropic compressibility. (d) Excess speed of sound. For sake of clarity, the error bars have not been plotted.

4.2. Kirkwood Buff Integrals and partial molar volumes

To investigate more deeply the non-idealities of a mixture, the partial molar volumes of components are very informative regarding the fluid behavior at the microscopic level [7]. To compute this quantity, the simplest method is to first fit the molar volume data at fixed pressure and temperature and then to analytically differentiate the fitted functions with respect to mole fraction [2-3], as done on our experimental data [1]. Nevertheless, this method is subject to high uncertainties due to the choice of the fitting functions and the number of mixture compositions close to the boundary conditions (x_{CO2} = 0 and 100 mol%). In particular, when applying the fitting method to data that may have large errors [55-57], e.g. systems near the critical point, it can result in inaccurate values of the partial molar volumes. During molecular simulations, partial molar volume can be directly computed from the Kirkwood and Buff Integrals (KBI), as described in Sect. 3.2, avoiding so the problem of the fitting procedure. Thus, we have

considered the latter method to determine the partial molar volumes of the two components in the studied mixtures.

To obtain the partial molar volumes from the Kirkwood-Buff theory [54], the KBI have been first computed by using the approach described in Sect. 3.2. Computed values of KBI are listed in Tables A. 5 - A. 7 of the Appendix. To validate these data, the isothermal compressibilities have been calculated from the Kirkwood-Buff theory by using these KBIs and compared to those obtained from the fluctuation theory, Eq. 8. Figure 9 displays such a comparison at the condition where κ_T varies the most strongly with the mole fraction (T=313.25 K, P=10.11 MPa). Results indicate that the two methods provide results consistent with each other, i.e. within error bars, which confirms the accuracy of KBI data.

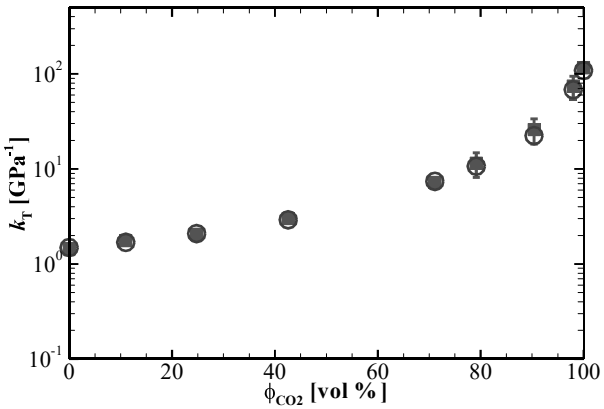

Figure 9. Comparison of molecular simulations results of isothermal compressibility of CO_2 + nC_7 mixtures at 313.25 K and 10.11 MPa computed from volume fluctuations (Solid squares) and the KB theory (Open circles).

Then, these KBI were used to calculate the partial molar volumes of CO_2 and n-heptane of the studied mixture at T=313.25 K and P=10.11 MPa thanks to the procedure described in section 3.2. For comparison, results of Kirkwood-Buff theory and experiments are together displayed in Fig. 10, showing a good agreement with each other. It appears clearly that the variations in the experimental partial molar volumes with mole fraction are fully consistent with those deduced from molecular simulations. In particular, the negative value of partial molar volume of n-heptane at infinite dilution is also predicted by the molecular simulations. These observations confirm the consistency in the partial molar volumes computed from experimental data and the chosen fitting procedure [1].

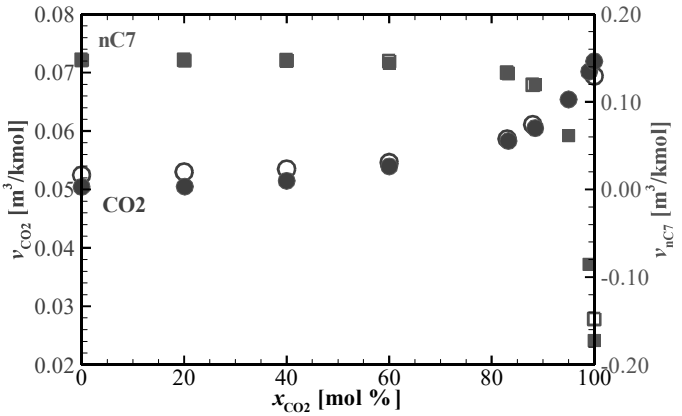

Figure 10. Partial molar volume of carbon dioxide (circles) and n-heptane (square) as a function of CO_2 mole fraction at T=313.25 K and P=10.11 MPa obtained from the fitting procedure on the experimental data (open symbols) and the Kirkwood-Buff theory combined with the molecular simulations (solid symbols).

4.3. Microscopic analysis of the cluster at infinite dilution of nC_7

Molecular simulations and experiments have both shown that the partial molar volume of n-heptane at infinite dilution is noticeably negative at T=313.25 K and P=10.11 MPa. Such unusual result has been interpreted as due to the formation of a cluster of CO_2 molecules around the nC_7 molecule, the so-called clustering effect [8-9]. This clustering phenomenon is often characterized and quantified by means of the excess number of CO_2 molecules surrounding the nC_7 molecule with respect to a uniform distribution at bulk density as [7]:

$$N_{CO2}^{excess} = \rho_{CO2}^{*} 4\pi \int_0^{\infty} [g_{CO2-nC7}^{\infty}(r) - 1] r^2 dr = \rho_{CO2}^{*} \cdot G_{CO2-nC7}^{\infty} \quad (31)$$

where the superscript ∞ refers to the infinite dilution and ρ_{CO2}^{*} is the density of pure CO_2. This excess number is also sometimes referred in the literature as the "cluster size".

Using the density ρ_{CO2}^{*} and the KBIs $G_{CO2-nC7}^{\infty}$ obtained from molecular simulation, N_{CO2}^{excess} is equal to 6.3±1.6. Such a positive value is the signature of an increase of the CO_2 density around the n-heptane molecule [8-9]. This value is in qualitative agreement with the value of 8 [1] that was computed from the experimental volumetric properties following the fluctuation theory developed in Ref. [7] as:

$$N_{CO2}^{excess} = \frac{RTk_{T,CO_2} - v_{nC7}^{\infty}}{v_{CO_2}} \quad (32)$$

The cluster size defined by Eq. 31 and Eq. 32 provides only an overall property of the cluster related to the excess number CO_2 molecules surrounding a nC_7 molecule relatively to a random distribution. Thus, to gain further microscopic insights on the cluster nature, MD simulations on mixtures close to the infinite dilution of nC_7 have been performed to estimate

the properties of the CO_2 molecules located in the region around the nC_7 where there is an excess of CO_2 molecules compared to a random distribution, as presented in the following sections.

A. Determination of the CO_2 molecules belonging to the cluster.

There exist many possible definitions to determine which molecules belong to a cluster [14, 16, 62-65]. The essence of these definitions is that the cluster is constituted of CO_2 molecules directly and indirectly "bonded" to the central nC_7 molecule [14, 62-63]. In this work, two molecules separated by a distance less than the radius of the first minimum of the corresponding RDF are considered to be directly bonded [64-65], whereas a molecule is considered to be indirectly bonded to a given molecule, if it is bonded to at least one molecule bonded to the given molecule [14].

In details, we have defined the molecules belonging to a cluster by two successive conditions. (i) All CO_2 molecules that are bonded directly and indirectly to the central nC7 molecule, using the criteria defined above, are collected. (ii) Then, are selected only those that are located within a spherical region surrounding the central nC_7 molecule [16], with a radius $R_{cluster}$ for which the RDF between nC_7 and CO_2 is nearly constant and equal to 1.0. Results shown in Fig. 11 indicate that this distance is around 30Å (i.e. nearly ten CO_2 molecular sizes). Hence, we have chosen $R_{cluster}$ to be equal to this value, i.e. $R_{clust} = 30$Å.

An illustration of this two-steps definition is shown in Fig. 12. The 1st to 10th CO_2 molecules are directly connected to the nC_7 molecule and so they are accounted for as belonging to the cluster. The 11th to 16th solvent molecules are indirectly connected to the nC_7 molecule, but only the 11th solvent molecule is considered to be in the cluster due to the added criterion of a limited region defined by $R_{cluster}$.

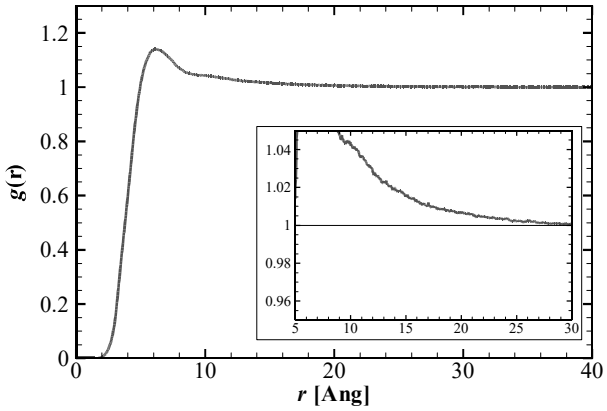

Figure 11. Radial distribution functions between CO_2 and nC_7 at infinite dilution ($x_{nC7} \rightarrow 0.0$) and $T = 313.25$ K and $P = 10.11$ MPa.

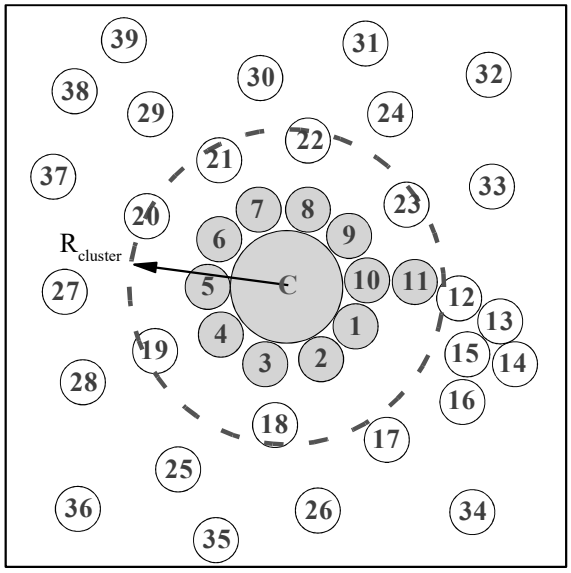

Figure 12. Schematic description of the definition of CO_2 molecules belonging to the cluster. Green large circle corresponds to the nC_7 molecule. Small grey circles are the CO_2 molecules belonging to the cluster. Small white circles are the CO_2 molecules that do not belong to the cluster.

B. Properties of CO_2 molecules belonging to a cluster

In a first step, the number $N_{\mathrm{CO2-cluster}}$of CO_2 molecules belonging to the cluster as defined in section 4.3.A, , was computed, using:

$$N_{\mathrm{CO2-cluster}} = \sum_i \delta_i \tag{33}$$

where $\delta_i = 1$ if the i^{th} CO_2 molecule belongs to the cluster and $\delta_i = 0$ otherwise. It should be emphasized that there is a simple link between the number $N_{\mathrm{CO2-cluster}}$, and the excess number of CO_2 molecule, N_{CO2}^{excess}, as:

$$N_{CO2}^{excess} = N_{CO2-cluster} - \rho_{CO2}^{*} V_{clust}\,, \tag{34}$$

where V_{clust} is the volume of the cluster.

Figure 13 depicts the variations of $N_{\mathrm{CO2-cluster}}$ with the time. It is shown that the number of CO_2 molecules belonging to the cluster region continuously fluctuates around an average value of 952±3.5, as shown in Fig. 14. Interestingly, the distribution of the fluctuations of the number of CO_2 molecules belonging to the cluster exhibits a Gaussian form with a standard deviation of 55±2.7 as shown in Fig. 14. This is a signature that the fluctuations are

mainly due to a continuous exchange between the CO_2 molecules of the cluster and those surrounding the cluster [15]. These results indicate so a weak nature of the cluster so defined.

In addition, assuming that the cluster is spherically symmetric and approximating its radius by $R_{cluster}$, one can deduce that $V_{clust} = (4\pi/3\, R_{cluster}^3)$. Using Eq. (34), we have obtained from the MD simulations $N_{\mathrm{CO2-cluster}}^{excess} = 4.6 \pm 3.5$ that is consistent with the value of $N_{CO2}^{excess} = 6.3 \pm 1.6$ given by Eq. 31. The difference is probably related to the fact that the volume of the cluster is overestimated when using $R_{cluster}$ as, by definition (section 4.3.A), not all CO_2 molecules located at a distance below $R_{cluster}$ from the nC_7 molecule belong to the cluster.

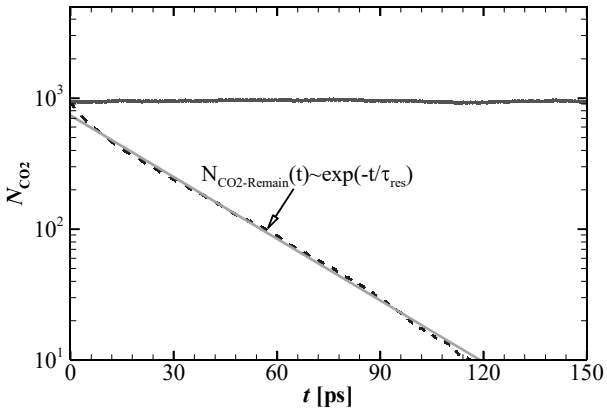

Figure 13. Variation of numbers of CO_2 molecules of the cluster with the time. (Red color) Solid line corresponds to $N_{CO2-cluster}$. (Blue color) Dashed-dotted line corresponds to $N_{CO2-remain}$.

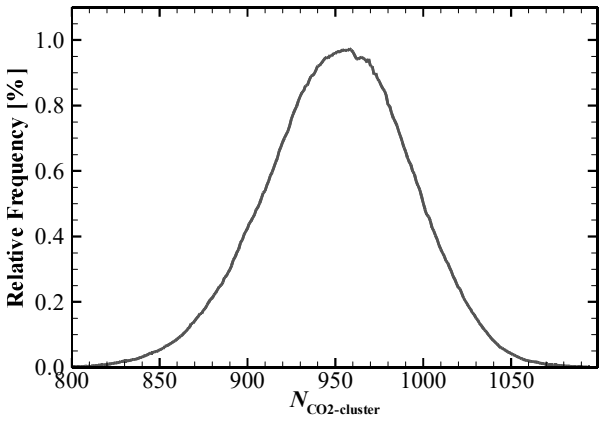

Figure 14. Relative frequency distributions of the number of CO_2 molecules of the cluster.

In addition, the stability of the cluster has been investigated by computing the residence time of CO_2 molecules belonging to a cluster [16]. More precisely, the residence time measures how long the CO_2 molecules reside in the cluster, and so how long it takes to the cluster to lose its identity. To compute this quantity, we have estimated the number of CO_2 molecules remaining in the cluster $N_{\mathrm{CO2-remain}}(t)$, during the time window 0 to t, which is defined as [16]:

$$N_{\mathrm{CO2-remain}}(t) = \sum_i \delta_i^0(t) \quad (34)$$

where, $\delta_i^0(t) = 1$ if the i^{th} CO_2 molecule resides in the cluster during the time interval [0, t], and $\delta_i^0(t) = 0$ otherwise. Fig. 13 displays the variation of $N_{\mathrm{CO2-remain}}$ with the time. Results show that $N_{\mathrm{CO2-remain}}$ exponentially decays with time, exhibiting a diffusive type behavior, which allows to deduce the residence time τ_{res} from the following equation [16]:

$$N_{\mathrm{CO2-remain}}(t) = N_{\mathrm{CO2-remain}}(t=0) \times \exp\left[-\frac{t}{\tau_{res}}\right] \quad (35)$$

By doing so, it is possible to deduce an average residence time of CO_2 molecules in a cluster $\tau_{res} = 27.5 \pm 1.5\mathrm{ps}$ which is of the same order of magnitude than the diffusion characteristic time [66] deduced from CO_2 diffusion coefficient [67]. This result further confirms the weak nature of the cluster and it diffusive behavior.

4.4. Effect of clustering on the macroscopic non-ideal behavior of the mixture

Indeed, clustering effect can be used to microscopically interpret the non-monotonic variation in the density with composition at T=313.25K and P=10.11MPa, see Fig. 15. To do so, it is easier to perform the interpretation by using molar density than mass density, to remove the effects of the molecular masses. Such a representation shows as well a non-monotonic variation of the molar density, see Fig. 15, but the maximum is reached at x_{CO2} around 95.0 mol% rather than at x_{CO2} around 85.0 mol% when using the mass density.

Qualitatively the interpretation of the data shown in Fig. 15 is the following. At infinite dilution of nC_7, i.e. when the CO_2 clustering effect is present, adding some nC_7 leads to the formation of more clusters which in turns leads to an overall increase of the density, as average density of CO_2 is higher in the cluster than in the bulk. This trend is confirmed by the negative value of the partial molar value of nC_7 for low nC_7 content, see Fig. 10. The molar density still increases by further adding nC_7, but the rate of increase is reduced because of the progressive overlapping of the clusters. At a certain value of nC_7 mole fraction, x_{nC7}≈5.0 mol% as shown in Fig. 15, the clusters tend to overlap more and more and so adding some extra nC_7 leads

progressively to a decrease of the molar density of mixture as the molar density of nC_7 is lower than that of the CO_2. The composition for which there is a change of behavior of molar density with composition is consistent with the change of sign of the partial molar value of nC_7 between x_{nC7}=1.0 mol% and x_{nC7}=5.0 mol%, see Fig. 10.

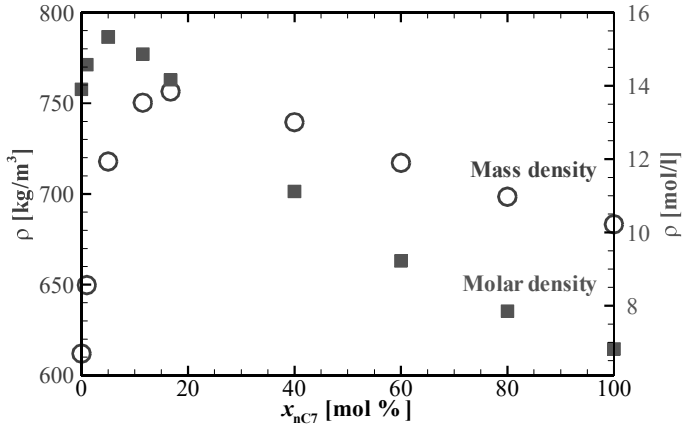

Figure 15: Dependence of density on the mole fraction of CO_2 at T=313.25K and P=10.11MPa. (Blue) Open circles correspond to the mass density. (Red) Solid squares correspond to the molar density.

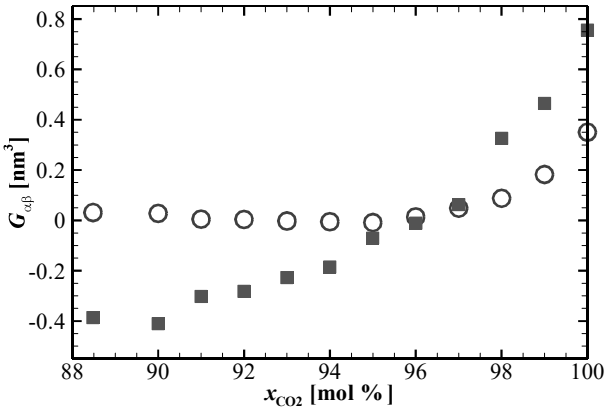

Figure 16: Comparison between the KBIs of the mixture at T=313.25 K and P=10.11MPa obtained from the molecular simulations at high CO_2 content. Circles correspond to the KBI of CO_2-CO_2. Squares correspond to the KBI of CO_2-nC_7.

Quantitatively, an analysis could be achieved using the values of the KBIs, which quantify the excess (or deficiency) of one species around another one relatively to a homogeneous molecules distribution, as follows. An addition of an infinitesimal amount of nC_7

to the pure CO_2 results in an increase of the molar density of the mixture as $G^{\infty}_{CO2-nC7} > G^{\infty}_{CO2-CO2}$, see the KBIs in Tables A. 5 – A. 7 of the Appendix. This increase should hold up to a mole fraction for which $G_{CO2-nC7} \approx G_{CO2-CO2}$. To confirm this expectation, we have additionally performed MD computations of the KBIs for CO_2 mole fraction varying from 90.0% to 99.0%. Results shown in Fig. 16 indicate that $G_{CO2-nC7} \approx G_{CO2-CO2}$ occurs at a CO_2 mole fraction around 96.0%, a value that is consistent with the one that can be deduced from the location of the maximum of the molar density, see Fig. 15, and with the change of sign of the partial molar value of nC_7, see Fig. 10.

V. Conclusion

This work forms the second part of a combined experimental [1] and numerical study of binary mixtures composed of carbon dioxide and n-heptane at two temperatures (303.35K and 313.25 K) and at pressures from 10 to 70 MPa. In this part, molecular simulations have been performed to investigate the thermodynamics and structural properties in order to complement the experimental results [1]. For that purpose, the Mie Chain Coarse Grained force field has been used to model carbon dioxide and n-heptane molecules and has been combined with Monte Carlo and Molecular Dynamics simulations.

In a first step, the thermodynamic properties including density, isothermal compressibility, speed of sound, isentropic compressibility and the corresponding excess properties obtained from Monte-Carlo simulations were systematically compared to those obtained from experiments. It has been found that the simulation results are fully consistent with the experimental ones, showing nevertheless larger deviations when approaching the critical point of CO_2 at high content of CO_2. Interestingly, one of the most peculiar behavior noticed experimentally, the non-monotonic variation of the density with the mole fraction of CO_2 at T=313.25K and P=10.11MPa, is very well captured by the molecular simulations.

In a second step, the Kirkwood-Buff theory has been used to directly compute the partial molar volumes of components from the simulations of the radial distribution functions. Interestingly, this direct method has provided results in good agreement with the experimental results. In particular, the noticeably negative value of partial molar volume of n-heptane at infinite dilution at T=313.25K and P=10.11MPa, computed indirectly from the experiment by a fitting procedure, was confirmed from molecular simulation results. Such a result confirms the occurrence of a clustering phenomenon in such conditions, i.e. CO_2 molecules tend to form a cluster around a nC_7 molecule, as deduced indirectly from volumetric experimental data. In

addition, the computed excess number of CO_2 was found to be in good agreement with the experimental indirect estimation.

To provide a microscopic picture of the clustering phenomenon, static and dynamic properties of the CO_2 cluster have been computed by molecular dynamics simulations at infinite dilution of nC7 at T=313.25K and P=10.11MPa. It has been found that the CO_2 molecules are affected by the presence of the nC_7 solute over a distance of about 3 nm (the clustering region). This corresponds to about 950 CO_2 molecules located in the cluster, a value two order of magnitude higher than the excess number of CO_2. Concerning the dynamic properties, the residence time of CO_2 molecules in the clustering region has been found to be diffusive like with an average value equal to about 25ps confirming the weak nature of the cluster.

Finally, thanks to the molecular simulations results and the Kirkwood-Buff Integrals, it has been possible to provide a microscopic explanation of the link between the clustering effect and the non-monotonic variation in the density with composition. Indeed, the increase of density with the mole fraction of n-heptane at high CO_2 content results from the clustering effect, as the number of CO_2 molecules surrounding a nC_7 molecule is larger than that surrounding a CO_2 molecule. Thus, adding n-heptane at low content of n-heptane increases globally the molar density of the mixture. This increase in density, which is reduced when the clusters overlap, holds up to a mole fraction for which $G_{CO2-nC7} \approx G_{CO2-CO2}$ that is corresponding to a mole fraction of CO_2 of about 96 %, consistently with the noticed change of sign of the partial molar volume of nC_7 for a similar composition.

Acknowledgements:

We gratefully acknowledge the "Communauté d'Agglomération de Pau-Pyrénées" for the PhD grant allowed to one of the authors, Abdoul Wahidou Saley Hamani. We would like to thank Pau University and the MCIA for providing computational facilities. Dr. Hai Hoang acknowledges financial support from the Vietnam National Foundation for Science and Technology Development (NAFOSTED) under grant number 103.01-2019.49

Appendix

In this appendix, density, isothermal compressibility, isentropic compressibility and speed of sound obtained from MC simulations are first presented. Then, the KBI computed by using the approach described in Sect. 3. 2., are provided.

Table A. 1: Density data of CO_2 + nC_7 obtained from MC simulations.

T (K)	P (MPa)	$\rho\ (kg.m^{-3})$ ± Error bars									
X_{CO2}/mol%		0.00%		20.14%		40.00%		60.00%		83.26%	
303.35	10.12	691.8	0.5	708.4	0.8	729.2	0.6	756.0	0.5	790.4	2.0
303.35	20.14	701.1	0.4	719.2	0.4	742.5	0.8	774.4	1.0	826.0	1.4
303.35	30.18	709.7	0.8	728.8	0.6	753.7	0.4	788.8	0.2	851.2	1.0
303.35	40.25	717.8	1.0	737.3	0.3	763.8	0.2	802.2	0.6	872.4	0.7
303.35	50.35	724	0.7	745.8	0.5	773.4	0.7	814.1	0.7	891.0	0.6
303.35	60.47	731.3	0.6	752.9	0.4	781.7	0.5	824.7	0.5	906.8	0.5
303.35	70.62	737.6	0.5	759.6	0.8	789.9	0.2	834.1	0.5	920.4	0.5
313.25	10.11	683	0.5	698.7	0.4	717.5	0.7	739.7	1.1	757.7	2.6
313.25	20.13	693.1	1.0	710.2	0.6	732	0.4	759.9	1.1	799.3	1.7
313.25	30.16	701.9	0.4	720.1	0.4	743.8	0.4	776.1	0.9	831.0	1.8
313.25	40.23	709.8	0.7	729.4	1.0	754.5	1.0	790.6	0.6	854.3	1.4
313.25	50.31	717.5	0.3	737.6	0.8	764.4	0.6	802.3	0.8	873.4	0.7
313.25	60.41	724.1	0.8	745.7	0.3	773.4	1.0	813.5	0.7	890.9	0.6
313.25	70.54	730.5	0.6	752.6	0.3	781.4	0.7	823.9	0.1	905.3	0.8
X_{CO2}/mol%		88.49%		95.00%		99.00%		100%			
303.35	10.12	792.9	4.6	784	3.9	772.2	4.1	760.9	8.1		
303.35	20.14	839.7	3.4	858.3	2.4	868.8	1.6	873	6.4		
303.35	30.18	870.2	3.1	898.5	3.1	923.2	1.5	927.3	2.0		
303.35	40.25	896.2	1.9	930.6	0.8	957.0	2.1	965.9	1.5		
303.35	50.35	916.4	0.1	955.8	0.8	985.9	2.0	996.2	1.5		
303.35	60.47	933.9	0.7	978	0.5	1011.0	0.9	1020	0.6		
303.35	70.62	949.5	1.0	996.4	0.6	1033.0	0.4	1043	0.2		
313.25	10.11	750.9	2.3	716.1	6.8	647.5	6.6	606.9	21.0		
313.25	20.13	809.4	3.4	822.2	4.1	820.2	3.6	819.7	3.6		
313.25	30.16	844.9	2.2	868.9	2.9	884.2	3.5	888.6	4.0		
313.25	40.23	874.3	0.6	901.7	2.5	925.8	1.0	932.5	1.5		
313.25	50.31	895.8	1.3	931.7	1.3	958.4	1.2	965.4	1.3		
313.25	60.41	915.9	0.5	955.1	1.4	985.4	0.4	993.4	1.1		
313.25	70.54	932	0.8	975.4	0.4	1008.0	1.2	1017	1.5		

Table A. 2: Isothermal compressibility data of CO_2 + nC_7 obtained from MC simulations.

T (K)	P (MPa)	$\kappa_T(GPa^{-1})$ ± Error bars									
X_{CO2}/mol%		0.00%		20.14%		40.00%		60.00%		83.26%	
303.35	10.12	1.485	0.101	1.583	0.069	1.945	0.167	2.550	0.184	5.048	1.137
303.35	20.14	1.249	0.029	1.380	0.066	1.635	0.131	2.176	0.111	3.699	0.471
303.35	30.18	1.199	0.074	1.211	0.053	1.386	0.094	1.722	0.104	2.381	0.192
303.35	40.25	1.108	0.079	1.061	0.088	1.230	0.073	1.471	0.078	2.109	0.568
303.35	50.35	0.980	0.058	1.025	0.052	1.115	0.052	1.340	0.087	1.834	0.098
303.35	60.47	0.851	0.059	0.876	0.039	1.005	0.031	1.202	0.069	1.711	0.114
303.35	70.62	0.780	0.048	0.891	0.038	0.929	0.040	1.071	0.024	1.399	0.083
313.25	10.11	1.439	0.090	1.762	0.044	2.053	0.142	2.994	0.167	7.204	0.472
313.25	20.13	1.365	0.070	1.447	0.045	1.742	0.077	2.328	0.088	4.335	0.515
313.25	30.16	1.187	0.053	1.282	0.093	1.514	0.041	1.972	0.124	3.136	0.338
313.25	40.23	1.108	0.066	1.149	0.039	1.442	0.047	1.631	0.106	2.159	0.255
313.25	50.31	1.049	0.061	1.083	0.031	1.237	0.045	1.365	0.061	1.978	0.066
313.25	60.41	0.949	0.020	0.960	0.046	1.100	0.040	1.272	0.057	1.752	0.082
313.25	70.54	0.882	0.041	0.890	0.072	0.992	0.025	1.130	0.078	1.549	0.087
X_{CO2}/mol%		88.49%		95.00%		99.00%		100%			
303.35	10.12	7.120	1.356	13.370	2.842	16.937	5.611	27.651	5.372		
303.35	20.14	4.192	0.322	5.824	0.592	7.168	0.631	7.578	1.132		
303.35	30.18	3.150	0.196	4.040	0.552	4.265	0.524	4.748	0.414		
303.35	40.25	2.536	0.397	2.868	0.190	3.122	0.100	3.309	0.126		
303.35	50.35	2.126	0.134	2.359	0.098	2.581	0.071	2.695	0.159		
303.35	60.47	1.781	0.103	1.966	0.061	2.089	0.150	2.266	0.056		
303.35	70.62	1.548	0.079	1.732	0.065	1.805	0.044	1.933	0.139		
313.25	10.11	11.473	3.313	25.939	7.663	74.370	19.951	116.3	13.5		
313.25	20.13	5.213	0.687	7.263	0.372	9.481	1.230	11.063	2.079		
313.25	30.16	3.915	0.421	4.461	0.280	5.575	0.788	5.567	0.442		
313.25	40.23	2.786	0.110	3.497	0.415	4.063	0.112	3.956	0.377		
313.25	50.31	2.352	0.158	2.733	0.093	2.959	0.106	3.191	0.169		
313.25	60.41	1.939	0.085	2.178	0.127	2.519	0.162	2.558	0.145		
313.25	70.54	1.676	0.100	1.816	0.063	2.088	0.034	2.153	0.097		

Table A. 3: Isentropic compressibility data of CO_2 + nC_7 obtained from Eq. 9 using the simulation data.

T (K)	P (MPa)	$\kappa_s(GPa^{-1})$ ± Error bars									
X_{CO2}/mol%		0.00%		20.14%		40.00%		60.00%		83.26%	
303.35	10.12	1.144	0.113	1.199	0.078	1.394	0.202	1.676	0.225	2.647	1.490
303.35	20.14	0.981	0.033	1.056	0.078	1.193	0.157	1.432	0.142	1.963	0.659
303.35	30.18	0.929	0.089	0.939	0.063	1.023	0.113	1.181	0.123	1.426	0.270
303.35	40.25	0.864	0.092	0.838	0.114	0.923	0.085	1.032	0.100	1.256	0.746
303.35	50.35	0.776	0.066	0.798	0.059	0.843	0.063	0.939	0.107	1.097	0.130
303.35	60.47	0.688	0.067	0.700	0.046	0.764	0.039	0.854	0.086	1.017	0.155
303.35	70.62	0.638	0.055	0.696	0.044	0.712	0.050	0.772	0.030	0.871	0.113
313.25	10.11	1.142	0.100	1.322	0.053	1.504	0.164	1.950	0.208	3.580	0.623
313.25	20.13	1.062	0.079	1.117	0.053	1.279	0.091	1.566	0.104	2.314	0.762
313.25	30.16	0.945	0.059	0.997	0.108	1.126	0.044	1.348	0.152	1.750	0.488
313.25	40.23	0.878	0.074	0.904	0.046	1.056	0.062	1.136	0.133	1.328	0.311
313.25	50.31	0.829	0.069	0.844	0.037	0.923	0.055	0.982	0.073	1.198	0.084
313.25	60.41	0.761	0.022	0.764	0.052	0.834	0.049	0.904	0.071	1.063	0.111
313.25	70.54	0.707	0.046	0.707	0.081	0.763	0.032	0.821	0.093	0.950	0.116
X_{CO2}/mol%		88.49%		95.00%		99.00%		100%			
303.35	10.12	3.337	1.897	4.660	4.827	5.188	4.069	6.871	10.070		
303.35	20.14	2.110	0.497	2.514	0.930	2.759	0.972	2.802	1.820		
303.35	30.18	1.643	0.268	1.812	0.818	1.802	0.814	1.871	0.594		
303.35	40.25	1.371	0.541	1.400	0.279	1.409	0.150	1.418	0.233		
303.35	50.35	1.164	0.188	1.191	0.145	1.193	0.109	1.207	0.242		
303.35	60.47	1.012	0.141	1.025	0.085	1.004	0.227	1.035	0.076		
303.35	70.62	0.896	0.106	0.907	0.092	0.887	0.062	0.902	0.203		
313.25	10.11	4.529	5.287	8.227	13.149	13.546	37.932	17.990	23.832		
313.25	20.13	2.591	1.034	3.065	0.503	3.538	1.950	3.810	3.407		
313.25	30.16	2.008	0.556	2.056	0.488	2.270	1.155	2.246	0.709		
313.25	40.23	1.507	0.140	1.674	0.606	1.760	0.229	1.699	0.560		
313.25	50.31	1.300	0.219	1.351	0.119	1.353	0.159	1.400	0.266		
313.25	60.41	1.108	0.121	1.132	0.180	1.161	0.252	1.178	0.220		
313.25	70.54	0.977	0.132	0.970	0.096	1.000	0.043	1.003	0.147		

Table A. 4: Speed of sound data of CO_2 + nC_7 calculated from Eq. 10 using the simulation data.

T (K)	P (MPa)	$w\ (m.s^{-1})$ ± Error bars									
X_{CO2}/mol%		0.00%		20.14%		40.00%		60.00%		83.26%	
303.35	10.12	1124.2	55.3	1084.9	34.5	992.0	71.6	888.4	59.4	691.3	193.7
303.35	20.14	1205.8	20.2	1147.6	42.2	1062.7	69.5	949.5	46.6	785.3	131.2
303.35	30.18	1231.9	58.0	1208.6	40.3	1139.0	62.6	1036.0	54.0	907.5	85.4
303.35	40.25	1270.1	66.9	1272.6	86.3	1191.2	54.4	1099.1	52.6	955.3	283.3
303.35	50.35	1334.5	55.8	1296.5	47.2	1238.1	45.5	1143.7	64.6	1011.3	59.8
303.35	60.47	1409.9	68.1	1377.5	44.7	1294.0	32.3	1191.4	59.8	1041.6	79.3
303.35	70.62	1457.3	62.2	1375.8	42.9	1333.7	46.6	1246.3	24.1	1116.9	71.9
313.25	10.11	1132.2	49.4	1040.5	20.6	962.6	51.9	832.5	43.7	607.2	51.8
313.25	20.13	1165.4	42.4	1122.9	26.0	1033.3	36.3	916.7	29.8	735.2	120.3
313.25	30.16	1228.0	37.8	1180.1	63.3	1092.6	21.2	977.6	54.4	829.2	114.8
313.25	40.23	1266.4	52.7	1231.2	30.6	1120.5	32.1	1055.3	61.5	938.8	109.1
313.25	50.31	1296.9	53.9	1267.1	26.9	1190.3	35.2	1126.5	41.1	977.4	33.9
313.25	60.41	1347.1	18.8	1325.2	44.7	1244.9	35.9	1166.3	45.0	1027.5	53.5
313.25	70.54	1391.8	44.8	1370.6	78.5	1295.1	26.4	1215.7	68.6	1078.1	65.4
X_{CO2}/mol%		88.49%		95.00%		99.00%		100%			
303.35	10.12	614.8	173.0	523.2	269.7	499.6	194.6	437.4	318.2		
303.35	20.14	751.2	86.9	680.7	124.9	645.9	113.2	639.4	205.3		
303.35	30.18	836.4	66.6	783.8	175.5	775.4	174.4	759.2	119.6		
303.35	40.25	902.2	177.0	876.3	86.9	861.1	44.9	854.3	69.5		
303.35	50.35	968.3	78.2	937.2	56.6	922.2	41.2	911.9	90.8		
303.35	60.47	1028.7	71.3	999.0	41.2	992.6	111.8	973.2	35.5		
303.35	70.62	1084.2	63.3	1051.8	53.2	1044.4	36.3	1030.9	115.9		
313.25	10.11	542.3	315.7	412.0	327.3	337.7	471.1	302.6	195.2		
313.25	20.13	690.5	136.3	629.9	50.1	587.0	160.5	565.9	251.8		
313.25	30.16	767.7	105.3	748.2	87.6	705.9	178.2	707.9	110.1		
313.25	40.23	871.1	40.2	813.9	146.3	783.5	50.5	794.6	130.4		
313.25	50.31	926.8	77.4	891.2	38.7	878.0	51.0	860.2	81.2		
313.25	60.41	992.5	53.9	961.5	75.6	934.9	101.1	924.3	85.8		
313.25	70.54	1047.9	70.4	1027.9	50.4	996.2	21.0	990.2	71.9		

Table A. 5: Kirkwood-Buff Integrals of CO_2-CO_2.

T (K)	P (MPa)	$G_{CO2\text{-}CO2}\,(nm^3)$ ± Error bars									
X_{CO2}/mol%		0.00%		20.14%		40.00%		60.00%		83.26%	
303.35	10.12	-	-	0.1440	0.0051	0.1344	0.0037	0.2820	0.0286	0.1340	0.0151
303.35	20.14	-	-	0.2986	0.0356	0.1066	0.0072	0.1447	0.0027	0.0740	0.0017
303.35	30.18	-	-	0.2226	0.0217	0.0771	0.0106	0.2229	0.0153	0.0646	0.0004
303.35	40.25	-	-	0.2087	0.0184	0.0797	0.0161	0.1194	0.0088	0.1120	0.0109
303.35	50.35	-	-	0.2290	0.0245	0.0731	0.0204	0.1868	0.0098	0.1235	0.0111
303.35	60.47	-	-	0.1426	0.0112	0.1143	0.0058	0.1130	0.0073	0.1516	0.0194
303.35	70.62	-	-	0.2891	0.0432	0.1346	0.0034	0.2680	0.0315	0.1159	0.0114
313.25	10.11	-	-	-0.0618	0.0397	0.0906	0.0105	0.1580	0.0082	0.1151	0.0144
313.25	20.13	-	-	0.1890	0.0185	0.2089	0.0165	0.1785	0.0096	0.0968	0.0072
313.25	30.16	-	-	0.1329	0.0057	0.1575	0.0046	0.1359	0.0008	0.0927	0.0082
313.25	40.23	-	-	0.1550	0.0026	0.1246	0.0039	0.1392	0.0014	0.0686	0.0040
313.25	50.31	-	-	0.0172	0.0176	0.1101	0.0056	0.1541	0.0085	0.1038	0.0119
313.25	60.41	-	-	0.2785	0.0513	0.1398	0.0099	0.1778	0.0125	0.0992	0.0081
313.25	70.54	-	-	0.3168	0.0535	0.2037	0.0174	0.1581	0.0047	0.0871	0.0073
X_{CO2}/mol%		88.49%		95.00%		99.00%		100%			
303.35	10.12	0.0509	0.0039	-0.0240	0.0002	-0.0098	0.0016	0.0129	0.0047		
303.35	20.14	0.0489	0.0025	-0.0249	0.0008	-0.0477	0.0008	-0.0525	0.0004		
303.35	30.18	0.0475	0.0044	-0.0203	0.0015	-0.0554	0.0000	-0.0597	0.0001		
303.35	40.25	0.0292	0.0003	-0.0280	0.0007	-0.0581	0.0001	-0.0623	0.0002		
303.35	50.35	0.0487	0.0037	-0.0231	0.0015	-0.0582	0.0002	-0.0630	0.0001		
303.35	60.47	0.0188	0.0036	-0.0239	0.0004	-0.0583	0.0003	-0.0627	0.0001		
303.35	70.62	0.0656	0.0077	-0.0157	0.0023	-0.0571	0.0000	-0.0625	0.0001		
313.25	10.11	0.0311	0.0016	-0.0087	0.0004	0.1823	0.0237	0.3503	0.0447		
313.25	20.13	0.0590	0.0086	-0.0355	0.0012	-0.0437	0.0007	-0.0427	0.0010		
313.25	30.16	0.0326	0.0020	-0.0326	0.0005	-0.0554	0.0001	-0.0558	0.0008		
313.25	40.23	0.0228	0.0019	-0.0301	0.0000	-0.0568	0.0004	-0.0625	0.0002		
313.25	50.31	0.0504	0.0065	-0.0305	0.0004	-0.0585	0.0000	-0.0632	0.0001		
313.25	60.41	0.0330	0.0027	-0.0243	0.0016	-0.0598	0.0005	-0.0635	0.0000		
313.25	70.54	0.0518	0.0063	-0.0332	0.0009	-0.0578	0.0002	-0.0631	0.0001		

Table A. 6: Kirkwood-Buff Integrals of CO_2-nC_7.

T (K)	P (MPa)	$G_{CO2\text{-}C7}\,(nm^3)$ ± Error bars									
X_{CO2}/mol%		Infinite dilution		20.14%		40.00%		60.00%		83.26%	
303.35	10.12	-	-	-0.0937	0.0007	-0.1221	0.0009	-0.2644	0.0159	-0.4575	0.0310
303.35	20.14	-	-	-0.1041	0.0032	-0.1120	0.0016	-0.1844	0.0008	-0.3239	0.0045
303.35	30.18	-	-	-0.0940	0.0015	-0.1032	0.0022	-0.2184	0.0082	-0.2921	0.0012
303.35	40.25	-	-	-0.0895	0.0010	-0.1005	0.0037	-0.1615	0.0042	-0.3575	0.0171
303.35	50.35	-	-	-0.0917	0.0020	-0.0986	0.0043	-0.1899	0.0046	-0.3665	0.0167
303.35	60.47	-	-	-0.0837	0.0009	-0.1052	0.0012	-0.1523	0.0036	-0.4044	0.0295
303.35	70.62	-	-	-0.0916	0.0027	-0.1080	0.0008	-0.2228	0.0149	-0.3434	0.0168
313.25	10.11	0.0773	0.0150	-0.0778	0.0032	-0.1156	0.0024	-0.2091	0.0059	-0.4605	0.0345
313.25	20.13	-	-	-0.0970	0.0018	-0.1364	0.0035	-0.2083	0.0056	-0.3781	0.0144
313.25	30.16	-	-	-0.0906	0.0001	-0.1242	0.0012	-0.1763	0.0003	-0.3518	0.0149
313.25	40.23	-	-	-0.0910	0.0008	-0.1128	0.0009	-0.1771	0.0013	-0.2949	0.0061
313.25	50.31	-	-	-0.0783	0.0008	-0.1082	0.0012	-0.1773	0.0039	-0.3438	0.0183
313.25	60.41	-	-	-0.0946	0.0038	-0.1116	0.0019	-0.1862	0.0060	-0.3297	0.0121
313.25	70.54	-	-	-0.0975	0.0041	-0.1231	0.0034	-0.1726	0.0017	-0.3041	0.0105
X_{CO2}/mol%		88.49%		95.00%		99.00%		Infinite dilution			
303.35	10.12	-0.3983	0.0086	-0.1919	0.0115	-0.0515	0.0127	-	-		
303.35	20.14	-0.3902	0.0094	-0.3063	0.0064	-0.2442	0.0046	-	-		
303.35	30.18	-0.3657	0.0118	-0.3342	0.0087	-0.1923	0.0121	-	-		
303.35	40.25	-0.3072	0.0006	-0.2862	0.0031	-0.2145	0.0049	-	-		
303.35	50.35	-0.3453	0.0082	-0.3052	0.0066	-0.2157	0.0065	-	-		
303.35	60.47	-0.2656	0.0098	-0.2975	0.0011	-0.2035	0.0094	-	-		
303.35	70.62	-0.3749	0.0180	-0.3463	0.0137	-0.2271	0.0032	-	-		
313.25	10.11	-0.3866	0.0110	-0.0701	0.0209	0.4651	0.0700	0.7559	0.2062		
313.25	20.13	-0.4372	0.0286	-0.2449	0.0052	-0.1823	0.0039	-	-		
313.25	30.16	-0.3454	0.0079	-0.2650	0.0033	-0.2032	0.0054	-	-		
313.25	40.23	-0.3009	0.0050	-0.2896	0.0000	-0.2782	0.0097	-	-		
313.25	50.31	-0.3591	0.0156	-0.2789	0.0017	-0.2331	0.0018	-	-		
313.25	60.41	-0.3093	0.0062	-0.3071	0.0091	-0.1883	0.0155	-	-		
313.25	70.54	-0.3473	0.0143	-0.2466	0.0062	-0.2307	0.0024	-	-		

Table A.7: Kirkwood-Buff Integrals of nC_7-nC_7.

T (K)	P (MPa)	$G_{C7\text{-}C7}\,(nm^3)$ ± Error bars									
X_{CO2}/mol%		0.00%		20.14%		40.00%		60.00%		83.26%	
303.35	10.12	-0.2345	0.0003	-0.2457	0.0004	-0.2572	0.0002	-0.2074	0.0094	0.2928	0.0674
303.35	20.14	-0.2321	0.0002	-0.2420	0.0006	-0.2568	0.0000	-0.2492	0.0004	-0.0227	0.0127
303.35	30.18	-0.2298	0.0002	-0.2407	0.0003	-0.2559	0.0002	-0.2292	0.0049	-0.0976	0.0044
303.35	40.25	-0.2278	0.0002	-0.2387	0.0003	-0.2539	0.0005	-0.2556	0.0015	-0.0007	0.0287
303.35	50.35	-0.2258	0.0002	-0.2361	0.0004	-0.2515	0.0006	-0.2402	0.0025	0.0071	0.0261
303.35	60.47	-0.2240	0.0002	-0.2346	0.0002	-0.2477	0.0001	-0.2556	0.0014	0.0666	0.0464
303.35	70.62	-0.2223	0.0002	-0.2324	0.0004	-0.2451	0.0002	-0.2199	0.0074	-0.0292	0.0259
313.25	10.11	-0.2371	0.0002	-0.2499	0.0000	-0.2617	0.0001	-0.2359	0.0049	0.4148	0.0892
313.25	20.13	-0.2345	0.0002	-0.2451	0.0005	-0.2544	0.0011	-0.2383	0.0038	0.1014	0.0313
313.25	30.16	-0.2321	0.0002	-0.2431	0.0002	-0.2534	0.0007	-0.2547	0.0006	0.0119	0.0289
313.25	40.23	-0.2297	0.0002	-0.2406	0.0004	-0.2536	0.0005	-0.2497	0.0015	-0.1032	0.0106
313.25	50.31	-0.2277	0.0002	-0.2391	0.0003	-0.2521	0.0000	-0.2487	0.0023	-0.0263	0.0297
313.25	60.41	-0.2259	0.0002	-0.2362	0.0005	-0.2491	0.0007	-0.2420	0.0032	-0.0507	0.0193
313.25	70.54	-0.2241	0.0002	-0.2339	0.0005	-0.2444	0.0010	-0.2466	0.0010	-0.0922	0.0164
X_{CO2}/mol%		88.49%		95.00%		99.00%		100%			
303.35	10.12	0.4597	0.0311	0.5377	0.0026	0.5103	0.0329	-	-		
303.35	20.14	0.3124	0.0364	0.5348	0.0631	1.9069	0.3033	-	-		
303.35	30.18	0.1721	0.0349	0.5765	0.0710	-0.6026	0.3108	-	-		
303.35	40.25	0.0022	0.0038	0.1837	0.0203	-0.2416	0.1062	-	-		
303.35	50.35	0.0834	0.0200	0.2542	0.0314	-0.3562	0.1848	-	-		
303.35	60.47	-0.1165	0.0254	0.2232	0.0036	-0.9160	0.3190	-	-		
303.35	70.62	0.1546	0.0438	0.5478	0.0875	-0.1048	0.1101	-	-		
313.25	10.11	0.7609	0.0801	1.3049	0.0894	2.7129	0.1729	-	-		
313.25	20.13	0.5062	0.0985	0.4773	0.0397	1.6688	0.2691	-	-		
313.25	30.16	0.1630	0.0302	0.2036	0.0006	0.4561	0.0630	-	-		
313.25	40.23	-0.0025	0.0171	0.2567	0.0079	1.7278	0.2969	-	-		
313.25	50.31	0.1226	0.0391	0.1596	0.0142	0.2187	0.0386	-	-		
313.25	60.41	-0.0046	0.0156	0.3026	0.0577	-1.1778	0.4613	-	-		
313.25	70.54	0.0858	0.0340	-0.0769	0.0395	0.1800	0.1103	-	-		

References

[1] J. -P. Bazile, D. Nasri, A. W. Saley Hamani, G. Galliero, J. -L. Daridon, Excess volume, isothermal compressibility, isentropic compressibility and speed of sound of carbon dioxide + n-heptane binary mixture under pressure up to 70 MPa. I Experimental Measurements, J. Supercrit. Fluids 140 (2018) 218.

[2] Assael, M. J.; Goodwin, A. R. H.; Vesovic, V.; Wakeham, W. A. Experimental Thermodynamics Volume IX: Advances in Transport Properties of Fluids, Royal Society of Chemistry: London (2014).

[3] Poling, B. E.; Prausnitz, M., O'Connell, J. P. The Properties of Gases and Liquids; Fifth Edition, McGraw-Hill (2004).

[4] P. Ehrlich, and R. Fariss, Negative Partial Molal Volumes in the Critical Region: Mixtures of Ethylene and Vinyl Chloride, J. Phys. Chem., 73 (1969) 1164.

[5] C. A. Eckert, D. H. Ziger, K. P. Johnston, and T. K. Ellison, The Use of Partial Molar Volume Data to Evaluate Equations of State for Supercritical Fluid Mixtures, Fluid Phase Equilib. 14 (1983) 167.

[6] C. A. Eckert, D. H. Ziger, K. P. Johnston, and S. Kim, Solute Partial Molar Volume in Supercritical Fluids, J. Phys. Chem., 90 (1986) 2738.

[7] P. G. Debenedetti, Clustering in Dilute, Binary Supercritical Mixtures: a Fluctuation Analysis, Chem. Eng. Sci., 42 (1987) 2203.

[8] D. B. McGuigan and P. A. Monson, Analysis of Infinite Dilution Partial Molar Volumes Using a Distribution Function Theory, Fluid Phase Equilib., 57 (1990) 227.

[9] J. F. Brennecke, P. G. Debenedetti, C. A. Eckert, K. P. Johnston, Letters to the Editor, AIChE J. 36 (1990) 1927.

[10] M. P. Allen and D. J. Tildesley, Computer Simulations of Liquids, Oxford University Press: New York (1987).

[11] D. Frenkel and B. Smit, Understanding Molecular Simulation: From Algorithms to Applications, Second Edition, Academic Press (2001).

[12] P. Ungerer, B. Tavitian, A. Boutin, Applications of Molecular Simulation in the Oil and Gasindustry, Technip (2005).

[13] K. E. Gubbins and J. D. Moore, Molecular Modeling of Matter: Impact and Prospects in Engineering, Ind. Eng. Chem. Res., 49 (2010) 3026.

[14] E. M. Sevick, P. A. Monson, J. M. Ottino, Monte Carlo Calculations of Cluster Statistics in Continuum Models of Composite Morphology. J. Chem. Phys., 88 (1988) 1198.

[15] I. B. Petsche, P. G. Debenedetti, Solute-Solvent Interactions in Infinitely Dilute Supercritical Mixtures: A Molecular Dynamics Investigation. J. Chem. Phys., 91 (1989) 7075.

[16] C. C. Liew, H. Inomata, S. Saito, Molecular dynamics study on solvent clustering in supercritical fluid solutions based on particle radial kinetic energy. Fluid Phase Equilib., 104 (1995) 317.

[17] M. Lagache, P. Ungerer, A. Boutin, A. H. Fuchs, Prediction of thermodynamic derivative properties of fluids by Monte Carlo simulation. Phys. Chem. Chem. Phys., 3 (2001) 4333.

[18] T. Kobayashi, J. E. S. J. Reid, S. Shimizu, M. Fyta, J. Smiatek, The properties of residual water molecules in ionic liquids: a comparison between direct and inverse Kirkwood–Buff approaches, Phys. Chem. Chem. Phys., 19 (2017) 18924.

[19] J. Milzetti, D. Nayar, N. F. A. van der Vegt, Convergence of Kirkwood–Buff Integrals of Ideal and Nonideal Aqueous Solutions Using Molecular Dynamics Simulations, J. Phys. Chem. B, 122 (2018) 5515.

[20] P. C. Petris, S. D. Anogiannakis, P. N. Tzounis, D. N. Theodorou, Thermodynamic Analysis of n-Hexane–Ethanol Binary Mixtures Using the Kirkwood–Buff Theory, J. Phys. Chem. B, 123 (2019) 247.

[21] N. Dawass, P. Krüger, S. K. Schnell, J. M. Simon, T. J. H. Vlugt, Kirkwood-Buff Integrals from Molecular Simulation. Fluid Phase Equilib., 486 (2019) 21.

[22] A. R. Leach, Molecular Modelling: Principles and Applications (2nd ed.). Harlow: Prentice Hall (2001)

[23] M. G. Martin and J. I. Siepmann, Transferable Potentials for Phase Equilibria. 1. United-Atom Description of n-Alkanes, J. Phys. Chem. B, 102 (1998) 2569.

[24] R. Aduri, B. T. Psciuk, P. Saro, H. Taniga, H. B. Schlegel and J. SantaLucia, AMBER Force Field Parameters for the Naturally Occurring Modified Nucleosides in RNA, J. Chem. Theory Comput., 3 (2007) 1464.

[25] S. W. I. Siu, K. Pluhackova and R. A. Böckmann, Optimization of the OPLS-AA Force Field for Long Hydrocarbons, J. Chem. Theory Comput., 8 (2012) 1459.

[26] Marrink, S. J.; Tielemanb, D. P. Perspective on the Martini model. Chem. Soc. Rev., 42 (2013) 6801.

[27] H. Hoang, S. Delage-Santacreu, G. Galliero, Simultaneous Description of Equilibrium, Interfacial, and Transport Properties of Fluids Using a Mie Chain Coarse-Grained Force Field. Ind. Eng. Chem. Res., 56 (2017) 9213.

[28] A. Mejia, C. Herdes, E. A. Müller, Force Fields for Coarse-Grained Molecular Simulations from a Corresponding States Correlation. Ind. Eng. Chem. Res. 53 (2014) 4131.

[29] G. Galliero, H. Bataller, J. P. Bazile, J. Diaz, F. Croccolo, H. Hoang, R. Vermorel, P.A. Artola, B. Rousseau, V. Vesovic, M. Bou-Ali, J.M.O. de Zarate, S. Xu, K. Zhang, F. Montel, A. Verga, O. Minster, Thermodiffusion in multicomponent n-alkane mixtures, Npj Micrograv., 3 (2017) 1.

[30] H. Hoang, P. Nguyen, M. Pujol and G. Galliero, Elemental and isotopic fractionation of noble gases in gas and oil under reservoir conditions: Impact of thermodiffusion, Eur. Phys. J. E, 42 (2019) 61.

[31] A. W. Saley Hamani, J. P. Bazile, H. Hoang, H. T. Luc, J. L. Daridon, G. Galliero, Thermophysical properties of simple molecular liquid mixtures: on the limitations of some force fields, J. Mol. Liq. (Revised manuscript with minor revisions submitted in Jan. 2020)

[32] E. Brini, E. A. Algaer, P. Ganguly, C. Li, F. Rodríguez-Ropero, N. F. A. van der Vegt, Systematic coarse-graining methods for soft matter simulations – a review. Soft Matter, 9 (2013) 2108.

[33] W. G. Noid, Perspective: Coarse-grained models for biomolecular systems. J. Chem. Phys., 139 (2013) 090901.

[34] G. Mie, ZurkinetischenTheorie der einatomigenKörper. Annu. Phys., 316 (1903) 657.

[35] E. A. Müller, L. D. Gelb, Molecular Modeling of Fluid-Phase Equilibria Using an Isotropic Multipolar Potential. Ind. Eng. Chem. Res., 42 (2003), 4123.

[36] K. S. Shing, K. E. Gubbins, K. Lucas, Henry Constants in Non-Ideal Fluid Mixtures. Mol. Phys., 65 (1988) 1235.

[37] A. Z. Panagiotopoulos, Direct determination of phase coexistence properties of fluids by Monte Carlo simulation in a new ensemble. Mol. Phys., 61 (1987) 813.

[38] A. Z. Panagiotopoulos, N. Quirke, M. Stapleton, D. J. Tildesley, Phase equilibria by simulation in the Gibbs ensemble: alternative derivation, generalization and application to mixture and membrane equilibria, Mol. Phys., 63 (1988) 527.

[39] B. Widom, Some Topics in the Theory of Fluids. J. Chem. Phys., 39 (1963) 2808.

[40] B. Widom, Potential-Distribution Theory and the Statistical Mechanics of Fluids. J. Phys. Chem., 86 (1982) 869.

[41] H. Kalra, H. Kubota, D. B. Robinson, H. J. Ng, Equilibrium Phase Properties of the Carbon Dioxide-n-Heptane System. J. Chem. Eng. Data, 23 (1978) 317.

[42] C. Avendaño, T. Lafitte, A. Galindo, C. S. Adjiman, G. Jackson, E. A. Müller, SAFT-γ Force Field for the Simulation of Molecular Fluids. 1. A Single-Site Coarse Grained Model of Carbon Dioxide. J. Phys. Chem. B, 115 (2011) 11154.

[43] T. Lafitte, A. Apostolakou, C. Avendaño, A. Galindo, C. S. Adjiman, E. A. Müller, G. Jackson, Accurate statistical associating fluid theory for chain molecules formed from Mie segments. J. Chem. Phys., 139 (2013) 154504.

[44] W. H. Press, S. A. Teukolsky, W. T. Vetterling, B. P. Flannery, Numerical Recipes in Fortran 77: The Art of Scientific Computing, 2nd Ed., Cambridge University Press (1992)

[45] R. Privat and J. N. Jaubert , Thermodynamic Models for the Prediction of Petroleum-Fluid Phase Behaviour, Crude Oil Emulsions- Composition Stability and Characterization, Editions InTech (2012).

[46] L. Verlet, Computer “Experiments” on Classical Fluids. I. Thermodynamical Properties of Lennard-Jones Molecules, Phys. Rev., 159 (1967) 98.

[47] H. J. C. Berendsen, J. P. M. Postma, W. F. van Gunsteren, A. Di Nola, J. R. Haak, Molecular Dynamics with Coupling to an External Bath, J. Chem. Phys., 81 (1984) 3684.

[48] H. C. Andersen, Rattle: A “Velocity” Version of the Shake Algorithm for Molecular Dynamics Calculations, J. Comput. Phys., 52 (1983) 24.

[49] Parris, P. Molecular Simulation Studies in the Supercritical Region, Doctoral thesis, University College London (2010).

[50] K. Saitow, D. Kajiya, K. Nishikawa, Dynamics of Density Fluctuation of Supercritical Fluid Mapped on Phase Diagram. J. Am. Chem. Soc., 126 (2004), 422.

[51] Y. Mishin, Thermodynamic Theory of Equilibrium Fluctuations, Ann. Phys., 363 (2005) 48.

[52] J. S. Rowlinson, F. L. Swinton, J. E. Baldwin, A. D. Buckingham, S. Danishefsky, Liquids and Liquid Mixtures: Butterworths Monographs in Chemistry, 3rd ed., Butterworth-Heinemann Ltd: London, Boston (1982).

[53] E. W. Lemmon, I. H. Bell, M. L. Huber, M. O. McLinden, NIST Standard Reference Database23: Reference Fluid Thermodynamic and Transport Properties-REFPROP, Version 8.0, National Institute of Standards and Technology, Standard Reference Data Program, Gaithersburg (2007).

[54] J. G. Kirkwood, F. P. Buff, The Statistical Mechanical Theory of Solutions. I. J. Chem. Phys., 19 (1951) 774.

[55] J. M. Stubbs, D. D. Drake-Wilhelm, J. I. Siepmann, Partial Molar Volume and Solvation Structure of Naphthalene in Supercritical Carbon Dioxide: A Monte Carlo Simulation Study. J. Phys. Chem. B, 109 (2005) 19885.

[56] N. N. Medvedev, V. P. Voloshin, A. V. Kim, A. V. Anikeenko, and A. Geiger, Culation of Partial Molar Volume and its Components for Molecular Dynamics Models of Dilute Solutions, J. Struct. Chem., 54 (2013) S271.

[57] M. Kohns, M. Horsch, H. Hasse, Partial molar volume of NaCl and CsCl in mixtures of water and methanol by experiment and molecular simulation, Fluid Phase Equilib., 458 (2018) 30.

[58] P. Ganguly, N. F. A. van der Vegt, Convergence of Sampling Kirkwood–Buff Integrals of Aqueous Solutions with Molecular Dynamics Simulations. J. Chem. Theory Comput., 9 (2013) 1347.

[59] S. K. Schnell, T. J. H. Vlugt, J. M. Simon, D. Bedeaux, S. Kjelstrup, Thermodynamics of small systems embedded in a reservoir: a detailed analysis of finite size effects, Mol. Phys. 110 (2012) 1069.

[60] P. Krüger, S. K. Schnell, D. Bedeaux, S. Kjelstrup, T. J. H. Vlugt, J. M. Simon, Kirkwood-Buff Integrals for Finite Volumes. J. Phys. Chem. Lett., 4 (2013), 235.

[61] A. W. Saley Hamani, Experimentation, Simulation and Modeling of Thermophysical Properties of Asymmetric Mixtures, Phd Thesis, University of Pau (2019).

[62] T. L. Hill, Statistical Mechanics: Principles and Selected Applications, Courier Corporation (1956).

[63] T. L. Hill, Molecular Clusters in Imperfect Gases. J. Chem. Phys., 23 (1955) 617.

[64] F. H. Stillinger, Rigorous Basis of the Frenkel- Band Theory of Association Equilibrium. J. Chem. Phys., 38 (1963), 1486.

[65] T. Ingebrigtsen, S. Toxvaerd, Contact Angles of Lennard-Jones Liquids and Droplets on Planar Surfaces. J. Phys. Chem. C, 111 (2007) 8518.

[66] E. L. Cussler, Diffusion: Mass Transfer in Fluid Systems, Cambridge University Press, New York (1997).

[67] G. Guevara-Carrion, S. Ancherbak, A. Mialdun, J. Vrabec and V. Shevtsova, Diffusion of methane in supercritical carbon dioxide across the Widom line, Sci. Rep. 9 (2019) 8466.